Rochester Institute of Technology
RIT Scholar Works

Theses | Thesis/Dissertation Collections

11-1-2002

Single wall carbon nanotube-nafion composite actuators

Brian Landi

Follow this and additional works at: http://scholarworks.rit.edu/theses

Recommended Citation
Landi, Brian, "Single wall carbon nanotube-nafion composite actuators" (2002). Thesis. Rochester Institute of Technology. Accessed from

This Thesis is brought to you for free and open access by the Thesis/Dissertation Collections at RIT Scholar Works. It has been accepted for inclusion in Theses by an authorized administrator of RIT Scholar Works. For more information, please contact ritscholarworks@rit.edu.

Single Wall Carbon Nanotube-Nafion Composite Actuators

Brian J. Landi

November, 2002

Thesis

Submitted in Partial Fulfillment of the Requirements for the Degree of Master of Science

Approved:

_____

Thesis Advisor, Thomas Gennett

_____

Department Head, Terence C. Morrill

Department of Chemistry

Rochester Institute of Technology

Rochester, New York 14623

Single Wall Carbon Nanotube-Nafion Composite Actuators

I, Brian J. Landi, hereby **grant permission** to the Wallace Library of the Rochester Institute of Technology to reproduce my thesis in whole or in part. Any reproduction will not be for commercial use or profit.

	11-20-02
Brian J. Landi	Date

Abstract

Single wall carbon nanotube (SWNT)-Nafion composite actuators have been demonstrated for 0.1 – 18 %, w/w doping of purified SWNTs within the polymer matrix. The high purity SWNTs, >95%w/w, were prepared using thermal oxidation and acid treatments for both in-house synthesized pulse laser vaporization SWNTs and commercially obtained HiPco material. Characterization of the purified SWNTs was performed using thermogravimetric analysis, scanning electron microscopy, optical absorption and Raman spectroscopy. Homogeneous dispersions of SWNTs in a Nafion polymer series were demonstrated using a combination of homogenization and high speed mixing techniques. Evaluation of SWNT-Nafion composites showed a "debundling" of the SWNT average bundle diameter when dispersed in the polymer matrix. Further analysis showed the efficient distribution of the high aspect ratio, conductive SWNT materials promoted actuation of the Nafion composite membrane to be reached at SWNT doping levels as low as 0.5% w/w. Utilizing a 2-electrode bimorph cantilever actuator immersed into an aqueous 1 M LiCl solution, tip deflections up to 4.5 mm were observed.

Table of Contents

List of Figures

List of Tables

Acknowledgement

I wish to thank my advisor, Tom Gennett, for all the support and direction during this thesis project. His guidance and tolerability were much appreciated, causing any future success and recognition I may receive in my scientific pursuits to be based on the solid foundation, which he fortified. I would also like to thank my pseudoadvisor/committee member, Ryne Raffaelle, who has begun the process of teaching me how to critically evaluate scientific data. Lastly, I wish to thank my other committee members, Dr. Andreas Langner and Dr. Michael Kotlarchyk, who were tremendous resources during the research process.

Above all, I wish to thank my parents and other family members who consistently support every endeavor I undertake. Also, I appreciate the friends and classmates who challenge me and allow for the development of long-lasting memories. Cheers!

1.0 Introduction

The development of electrochemical sensors and actuators has been a recent area of study, with preliminary advancements in artificial muscle and micro-electromechanical systems (MEMS) technologies. An electrochemical actuator is defined as a device that converts synergistic electrical and chemical processes to produce a mechanical response. The mechanical response typically resembles a bending or flexing of the actuating material, resulting from the electrochemical excitation.[1] These devices have potential applications in medicinal procedures like arterial bypass surgery, where delicate catheter insertion and manipulation is critical to success. Other developments for medicine may come from microactuators being applied to artificial muscle research. Another field that is optimistic for actuator development is optics, where microactuators may be employed for positioning of mirrors or lenses. Additionally, it has been proposed that aircraft will be constructed with "microflaps" that improve drag properties for enhanced landing.[2] Regardless of the many scientific applications for actuators, it is imperative for researchers to evaluate and characterize the necessary properties that allow for successful technological integration.

Studies designed to evaluate actuation properties specific to conducting polymers, carbon nanotubes, and ion-exchange polymer metallic composites (IPMCs) have been reported by many groups in the literature.[2-6] The most prominent conducting polymers are polypyrrole[3,4] and polyacetylene.[2] Controlled variations of redox reactions on the polymer backbone account for the observed actuation.[2-4] Work done by Baughman et. al., has initiated the analysis of carbon nanotubes as actuating devices, operating via a non-Faradaic mechanism.[5] Another very popular area for thin film polymeric actuators has been the analysis of metal-doped Nafion actuators, which function via ion intercalation and osmotic effects.[6] Although each of these systems operates

under different conditions and mechanisms, the overall goal is to produce a highly efficient actuator for device application.

In this thesis project, a series of single wall carbon nanotube (SWNT)-polymer composites is evaluated to identify potential polymer electrode films that are suited for actuator development. An SWNT-Nafion actuator has been developed and characterized using common mechanical analyses. The series of uniform composites was prepared by dispersing purified SWNTs with varying weight percents into the Nafion polymer matrix, followed by solution casting, allowing for analysis of the physical properties in each respective film. Instrumental analysis of SWNTs and SWNT-Nafion composites was performed using optical spectroscopy, thermogravimetric analysis (TGA), and scanning electron microscopy (SEM). Quantification of each bimorph cantilever actuator (device responsive to changes in opposite electrode expansion when electrically stimulated) was achieved using displacement analysis via an optical lever apparatus. The results display a novel, characterized actuating device based on an SWNT-polymer composite that achieved significant displacements.

1.1 Electrochemical Actuators

Construction of electrochemical actuators consists of three components: anode, cathode, and electrolyte. Ionic species are transported through the electrolyte intercalating at the anode and cathode to satisfy either oxidation and reduction (redox) reactions or establish electric double layers, producing faradaic and non-faradaic processes, respectively. The charge transfer initiates dimensional changes in the actuator electrodes, producing axial strain (Δ Length/Length), and a corresponding macroscopic deflection. Electrochemical actuators are different than other actuator types like electrostatic and piezoelectric, since an applied voltage stimulates the operation rather than an electric field. This provides a significant advantage for electrochemical actuators

since only a few volts or less are needed to produce work responses that are an order of magnitude greater than electrostatic or piezoelectric ones.[2]

Electrochemical actuators satisfy many of the ideal properties necessary for development of artificial muscle or MEMS devices, but also contain several disadvantages. Shahinpoor highlights several key factors which are required for micromanipulation: (1) flexible material, (2) long cycle life, and (3) fast, simple reaction mechanism.[7] More specifically, actuator electrodes should be thin, with minimal inner electrode separation, to promote higher rates of diffusion for ionic intercalation. Also, surface effects should minimize electrode resistance to enhance electrical stimulus. Electrolyte selection requires ionic species, which have high mobility to maintain fast transfer rates between electrodes in the faradaic actuators. Baughman has cited these characteristics as dominating factors in the large work per cycle and force values obtained for conducting polymer actuators and polymeric gel actuators, respectively. While electrochemical actuators exemplify many key features, there are several limitations that require attention. Most importantly is the necessity of an electrolyte solution, discouraging any attempts for solid-state structures. Some attempts however, are being directed towards use of a solid electrolyte, like hydrated poly(vinyl alcohol)/H_3PO_4.[2] A second observed shortcoming is the limited cycle life of the electrochemical actuators largely attributed to the doping/dedoping effects of ion intercalation for faradaic actuators.[2] A disadvantage shown for IPMC actuators is delamination of the surface metal coating such as gold on polypyrrole[2] or platinum on poly(acrylnitrile)[8] that is responsible for actuation at high voltages. While these characteristics outline important guidelines for actuator development, consideration of several types, namely conducting polymer, gel fiber and ionic conducting Nafion, can in turn provide further understanding.

Substantial work has been done to evaluate the electrochemical properties of gel, conducting polymer, and IPMC systems. The reports show encouraging developmental results, but each

varies substantially between polymer type, electrolyte selection, pH, and excitation voltages. It is the purpose of this section to outline the current state of field for these actuator systems, describing the reported values as a means of comparison for carbon nanotube actuators and potential SWNT-polymer composite actuators.

Polyelectrolyte gels are unique in that under an electric field, they swell in volume inducing a mechanical change. A recent report using poly(acrylonitrile) (PAN) gel fibers exhibited swelling when exposed to alkaline media and contraction during acidic conditions. These gel fibers deposited with platinum or intercalated with graphite fibers, produced an approximately 40-50% elongation after 10 minutes of electrical activation.[8] These values are considerably higher than polythiophene, which was shown to expand by only 2% after 20 minutes.[9] Although the PAN gel systems produced considerable strain, slow reaction times and high voltages (10-20 V excitation) display inferior properties to other actuator systems.[8] Better performance systems have been observed with conducting polymers like polypyrrole[3,4] and polyacetylene.[2] These conducting polymers operate through redox reactions, causing length changes in the carbon-carbon bonds on the polymer backbone. Electrolyte and charge density effects have also been cited as potential mechanistic factors for conducting polymer actuators.[3] Film expansion values for these films have been reported to equal 3% for polypyrrole[4] at neutral pH and 1.6% for alkali-doped polyacetylene films.[2] While the ionic dopant species has been shown to be a critical parameter during actuation, solvent effects are reported to be just as significant. Osmotic effects have been proposed to significantly alter the degree of actuation in conducting polymers by increasing film expansion upon decreased electrolyte concentration. Bay et. al., attribute this result to the influx of water into the polymer films from the high ionic strength of the doped polymer matrix.[3] This study supports the significance of the internal electrochemical redox reactions at the polymer backbone and shows that normalization of electrolyte concentrations is critical for comparison of different

conducting polymer systems.[3] While attempts to develop actuators using conducting and gel polymers have been realized, increased response rates, higher cantilever deflection limits, and lower operating voltages have been characteristically shown for the ionic polymer Nafion.

The perfluorinated ionomeric polymer, Nafion® (Figure 1), has been shown to actuate under electrical stimulus in an electrolyte solution when doped with significant amounts of metal. The prominent structural model for Nafion considers a hydrophobic region with the fluorocarbon backbone and interstitial channels with ionic clusters that contain sulfonate groups (Figure 2). The micellular-like ionic clusters have sulfonate groups with bound H_2O and counterions, usually H^+ or Na^+. While the interstitial channels have some H_2O present, mostly it is void volume. Variations in morphology for these locations, the ionic clusters and interstitial channels, is directly affected by the cation charge bound to the sulfonate.[10]

Actuation using Nafion in aqueous electrolytes has been performed routinely upon surface metal doping, typically platinum or gold, at concentrations >3 mg/cm^2.[5,8] Abe et. al., first showed the effects of counter cation species in the electrolyte, concluding that Li^+ produced the largest displacement, ~1 mm towards the anode. The mechanism provided for this electrochemical actuation supports the bending and relaxation processes observed. Upon electrical excitation (a few volts or less), the hydrated counter cation moves to the cathode side of the electrode, swelling the composite with water, and inducing a bend in the film towards the anode. After prolonged electrical excitation of the film, there is an observed relaxation or creeping process back towards the cathode side. Osmotic effects have been cited as the source of this occurrence. Therefore, the presence of water has an astounding impact on the overall mechanism.[6]

Improvements to the actuation process, namely enhanced load capability, larger displacements, and surface modifications, have been the focus of recent work.[11,12] Film thickness effects on load capability have shown that doubling the thickness for each Nafion film corresponds

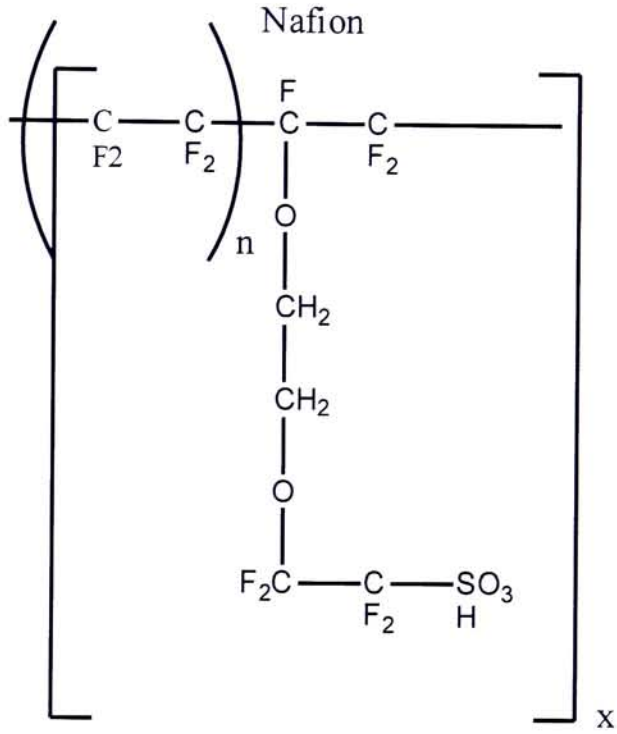

Figure 1: Structure of Nafion.®

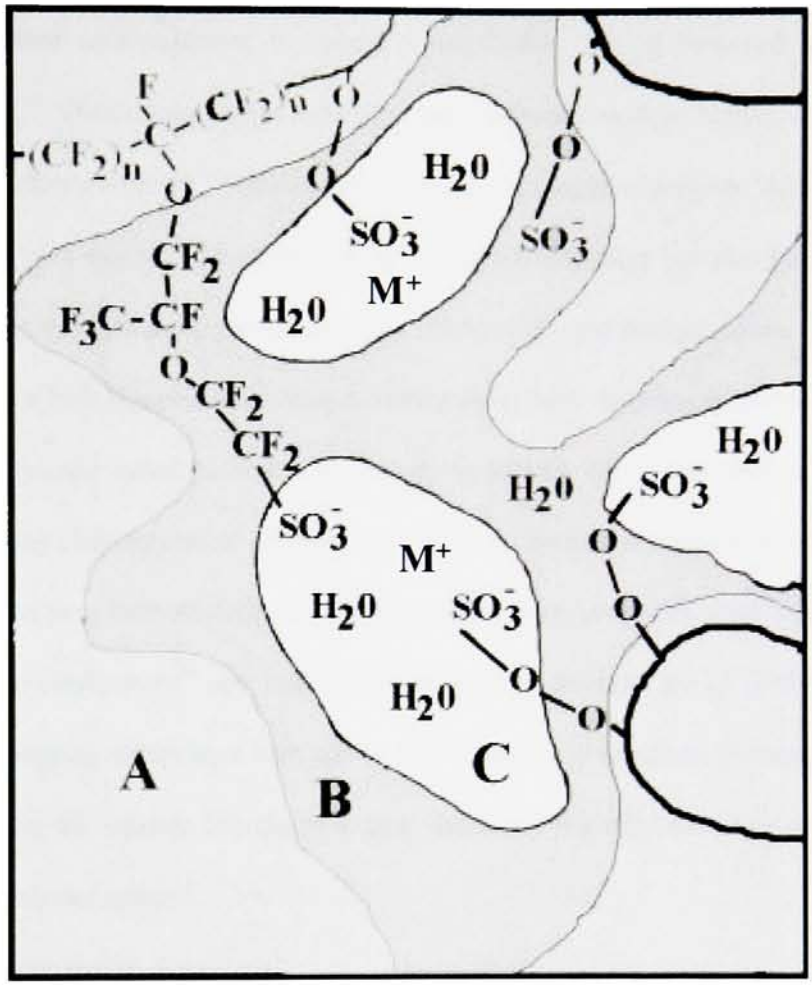

Figure 2: Structural model of Nafion depicting polar ionic cluster regions and a nonpolar backbone. In the diagram, (A) is the hydrophobic fluorocarbon, (B) is the interstitial void volume, and (C) is the hydrated ionic cluster comprising a sulfonate and cation (M^+ -typically H^+ or Na^+).

to an 8-fold increase in force generated.[11] While commercially available films are ~200 μm, Shahinpoor et. al., have developed a procedure to produce 2 mm thick Nafion films.[11] Another group has evaluated the metal doping characteristics of Nafion films by roughening the surface to increase surface area sufficient to enhance platinization for an observed 50% increase in displacement.[12] While platinum has been the traditional metal to dope Nafion, other reports have investigated effects of gold,[13,14] and copper-platinum,[15] as superior dopants. Although the surface effects have been studied in considerable detail, significant effort has also been made towards understanding the H_2O and ionic conductivity effects within the Nafion matrix. Nafion has been shown to have both bound and non-bound water present, with the amounts and ratios varying with the type of counter cation present. The ability to hydrate the counter cation, especially as it migrates during electrochemical actuation, is a property distinct to each cation. Electrolytes with lithium cations have been shown to exhibit the best actuation properties. This can be attributed to the high ionic conductivity[16] and large hydration spheres observed for Li^+ in the Nafion matrix.[6] Although promising results have been shown for Nafion-based actuators, the necessity to have ion intercalation at the cathode introduces a time deficiency for migration, similar to the gel and conducting polymer systems.

1.2 Carbon Nanotube Actuators

Demonstration of carbon nanotube actuators in 1999 by Baughman et. al., displayed a novel material for conversion of electrical energy into mechanical energy. Preliminary results predicted the highest work capacity of known actuating materials.[5] The single wall carbon nanotube devices were constructed using strips of "buckey paper" sheets assembled from as-produced laser-generated material. Each strip was placed on opposite sides of an insulating piece of double-stick tape and the carbon nanotube electrodes were connected to clamped platinum electrical leads. The device was inserted in a 1M NaCl solution and several volts were applied, producing

deflection at the cantilever tip up to about a centimeter (Figure 3). Further characterization showed that the bimorph cantilever actuator produces strain results which are >0.2%. This value already exceeds the highest strain value of ~ 0.1% known for ferroelectric ceramics. Theoretical predictions indicate that carbon nanotube actuators can potentially reach strain values of ~1% when the carbon nanotubes exist as individual SWNTs, i.e. not bundled. The initial work showed surface area measurements using the Brunauer-Emmett-Teller (BET) method of the buckeypapers to be ~300 m^2/g, whereas individual SWNTs are predicted to have values of ~1600 m^2/g.[5] This correlates with the five-fold decrease of observed strain versus the theoretical values based on surface area assignments. A result that is explained by only the exterior SWNTs in the bundles participating in the actuation (Figure 4), highlighting an important observation to support the mechanism for actuation. It was concluded that the actuation in carbon nanotubes is caused by charge injection from the electrolyte salt present in solution, promoting an electric double layer.[5] In turn, the charge induces quantum mechanical expansion of the covalent framework of the carbon nanotubes, producing an observed strain. Therefore, a larger degree of actuation was proposed for debundled SWNTs, resulting from an increased surface area, thereby enhancing electric double layer effects. Overall, the initial study by Baughman et. al., has displayed the extreme potential for carbon nanotube actuators and provides a preliminary understanding of the mechanism which supports this technology.[5]

There have been a number of recent reports describing potential applications of carbon nanotube actuators. An example is the pneumatic response for carbon nanotube buckey papers due to gas formation between carbon nanotube layers, also shown by Baughman et. al.[17] Results indicate >2% contraction of the carbon nanotube sheets when exposed to a 5M NaCl solution and voltages between +0.5 and +1.5 V. Although these results are impressive, the requirement to develop consistent carbon nanotube paper layers to form reproducible pneumatic actuators with

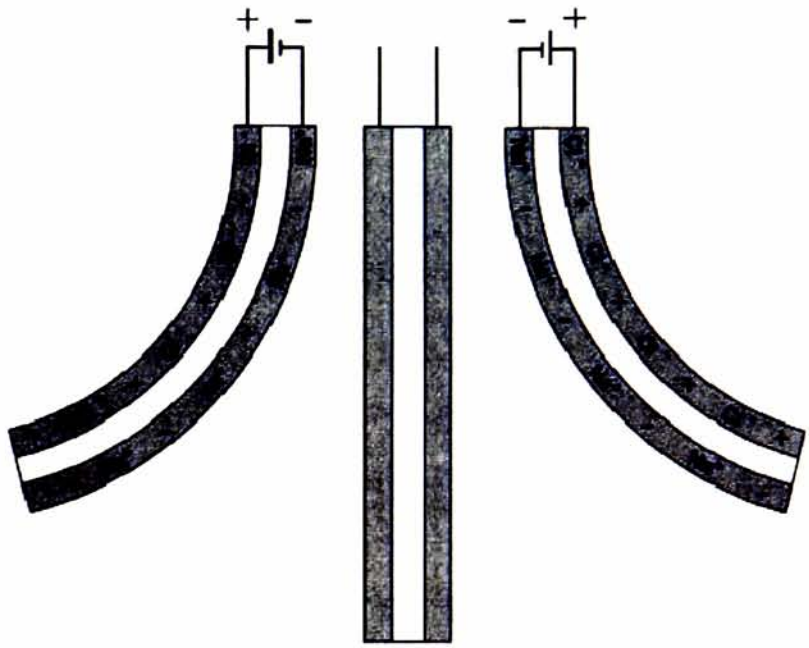

Figure 3: Representation of the bimorph cantilever actuator deflection reported for carbon nanotube actuators.

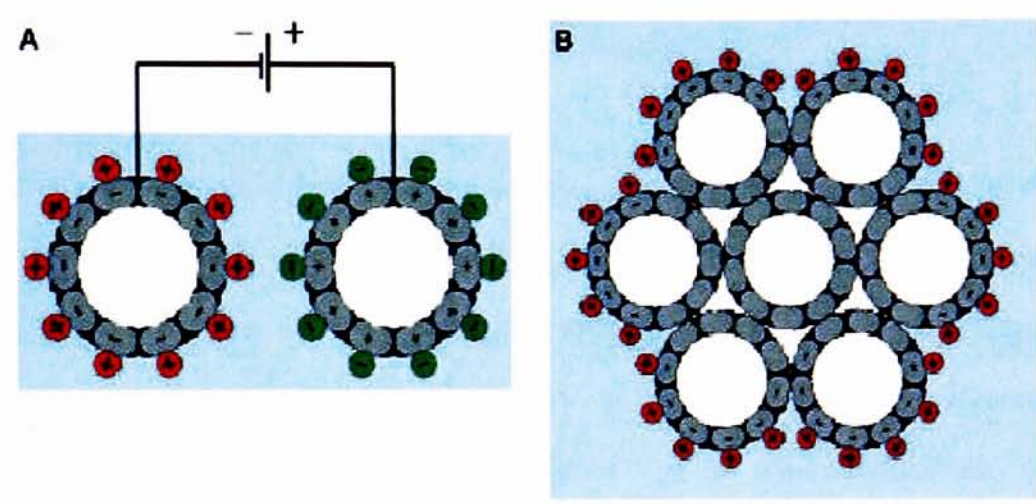

Figure 4: Electric double layer effects reported for carbon nanotube actuators of (A) individuals SWNTs, and (B) bundled SWNTs.

long life cycles is limiting.[17] Other attempts to study the actuation properties of individual SWNTs has been fraught with difficulties, although some success has been achieved growing carbon nanotubes across pre-trenched wafers using the CVD process, and monitoring potential actuation using an Atomic Force Microscopy (AFM) tip.[18] Additional attempts are being made to develop "nanotweezers," where individual SWNTs bound to an AFM tip under an applied dc voltage cause the two carbon nanotubes to approach each other. Such techniques may be applicable to the development of manipulating structures for nanoelectronics.[19]

1.3 Carbon Nanotubes

Each type of carbon nanotube, single wall or multi-wall, exhibits unique and useful properties for both basic science and applied technology. Although SWNTs are the focus of this thesis project, a brief overview of the properties of multi-wall carbon nanotubes (MWNTs) will be described to highlight the differences between the two types. MWNTs are composed of concentric layers of graphene sheets stabilized by Van der Waal's interactions. Observed MWNT diameters range from 2 - 25 nm, lengths are ~1 micron, and spacing between coaxial layers equal 0.34 nm.[20] Synthesis of MWNTs is primarily performed by arc-discharge techniques,[21] while alternative methods using quartz substrates produce similar quality and yield.[22] Structural rigidity of MWNTs plays a key role in polymer composite studies, evident from Jin et. al., to physically align MWNTs within a polymer matrix by mechanical stretching.[23] Structural properties of MWNTs include the ability to be twisted and "kinked," before elastically returning to original shape. Research indicates that these kinks may potentially lead to functionalization of the carbon nanotube sidewalls, increasing chemical reactivity.[24] The conduction mechanism in MWNTs is under debate since results supporting both ballistic and diffusive currents have been reported.[21] The discrepancies may be attributed to the varying helicities of carbon nanotube layers in a MWNT, thereby showing both types of conduction occur dependent on carbon nanotube

formation. Work by de Heer et. al., has shown that conduction in a MWNT occurs only on the most external layer, indicating primarily structural support by internal layers.[25] Multi-wall carbon nanotubes are also being used as fundamental demonstrations for the Aharonov-Bohm effect,[26] field and light emission properties,[21] and tip "sharpening" by Scanning Tunneling Microscopy for potential nano-scale probes.[27]

1.4 Single Wall Carbon Nanotubes

Although MWNTs have several key applications, this thesis focuses on the properties and applications of single wall carbon nanotubes (SWNTs). The structure of SWNTs is best imagined when looking at a single sheet of graphite (graphene) and rolling the sheet such that the edges match. Each generated tube incorporates hexagonal benzene rings along the cylindrical shaft, carbon atoms being sp^2 hybridized. The carbon nanotube caps include pentagon rings to create the closed end with half of a buckeyball (Figure 5).[28] Therefore, a carbon nanotube of C_{60} character (containing 12 pentagons and 20 hexagons) can be imagined as an expansionary growth within the fullerene that leads to a long, cylindrical structure for stability. The manner in which the benzene rings orient along the nanotube structure determines the unique chirality-types associated with carbon nanotubes.[20] Chirality is described by the roll-up vector for carbon nanotubes from a graphene sheet. Representation of this vector for SWNTs is depicted by the following (Figure 6):[20] $C_h = n\,a_1 + m\,a_2$; where a_1 and a_2 are lattice vectors, n and m are integers; and the symmetry for the carbon nanotube is directly related to the unit (n,m).[29] Figure 6 indicates two unique SWNT chiral types represented by dashed lines at 0° and 30°, (n,0) zigzag carbon nanotubes and (n,n) armchair carbon nanotubes, respectively. All other symmetry operations between these two will be termed chiral carbon nanotubes and their properties will vary based on helicity. Theory indicates that armchair carbon nanotubes are metallic, while zigzag and chiral

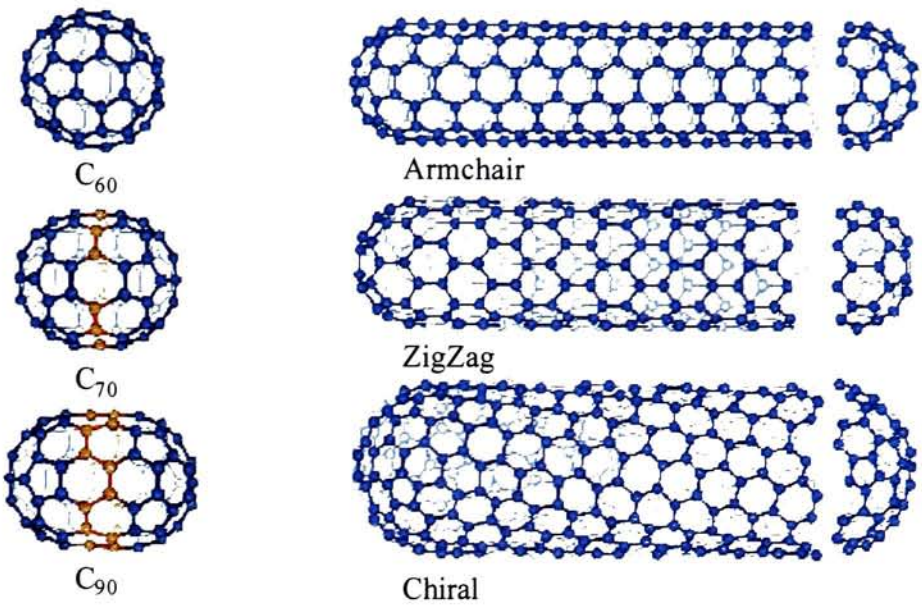

Figure 5: Structural representations of fullerenes and single wall carbon nanotubes, displaying variation in size for the fullerene endcaps of single wall carbon nanotubes and arrangements of the hexagons in the single wall carbon nanotubes to produce different helicities.

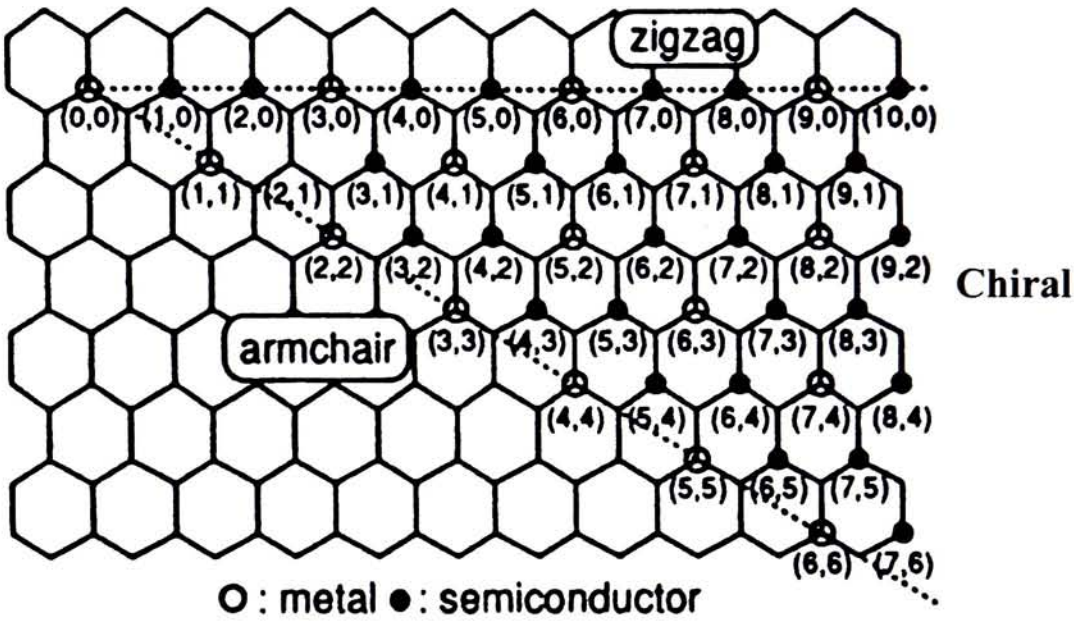

Figure 6: Symmetry elements for SWNTs depicting the chiral designations for the (n, m) vector. Each chirality represents a unique SWNT that corresponds to a certain diameter and electronic structure. The points with open circles represent metallic SWNTs whereas closed circles are for semiconducting.

carbon nanotubes are semiconducting unless through symmetry (n-m)/3 = integer, then they also will be metallic (see Figure 6).[29]

1.5 Structural and Electronic Properties

Derived from their symmetry, SWNTs exhibit various diameters, corresponding with unique structural and electronic properties. SWNTs produced by certain synthetic procedures can produce diameters as low as 0.7 nm, equivalent to the C_{60} cap.[30] Most laser grown SWNTs exhibit diameters of ~1.2-1.4 nm,[31] representative of a C_{240} cap.[20] Recent work by three independent groups has reported stable synthesis of the smallest diameter SWNT, ~ 0.4 nm.[32-34] The chirality of the 0.4 nm SWNT is uncertain with one group reporting a (3,3) armchair[34] and another a (5,0) zigzag SWNT.[32]

As stated above, armchair and chiral SWNTs with symmetry equal to (n-m)/3, exhibit metallic properties.[29] Conduction in these structures follows a ballistic nature, with theoretical predictions of a perfect conductor having a value of $4e^2/h$ (where e is electron charge, and h is Planck's constant); with groups reporting 25-50% of this value. Additional "quantum dot" studies can elucidate electron activity in metallic SWNTs by measuring the conductance vs. gate voltage, to determine whether conducting oscillations exist from ordered electronic states along the length of the tube. Results show that electrons can travel up to 10 μm before electron scattering distorts the regular oscillations.[35] Consequently, conductance values for SWNTs have been reported to equal 10^4 S/cm,[5] with current capacities 1000 times that of a copper wire.[36]

Single wall carbon nanotubes not displaying metallic symmetry offer a different set of properties, closely resembling silicon in standard p-type metal-oxide-silicon field-effect transistor (MOSFET) applications. These semiconducting SWNTs can be used as transistors, where application of a negative bias causes conduction via hole carriers. Researchers indicate that adsorbed species on the SWNT surfaces cause this p-type doping,[35] while in certain instances,

atoms like potassium can orient to donate electrons to the SWNT, changing doping to n-type.[37] Overall, SWNTs offer tremendous potential for electronic applications, each directly related to the unique properties exhibited by both metallic and semiconducting SWNTs during synthesis.

In addition to electronic properties, SWNT structure and sample morphologies are also being widely investigated. It has been shown that SWNTs typically exist in bundles after purification (Figure 7). Work by Gennett et al, has shown development of pure "superbundles" with diameters ranging up to 1μm.[38] The resulting space between SWNTs in bundles is caused by Van der Waal's interactions between individual SWNTs. The reported value for SWNT spacing in bundles is 0.315 nm, approximately equal to the distance between graphene sheet layers in graphite, 0.335 nm.[20] Individual SWNT physical characteristics are of intense interest due to their unique properties, and potential for composite applications. The high aspect ratios for the SWNTs, i.e., nano-diameters versus micron-lengths, suggest utility as reinforcements in polymer and ceramic composites.[39] In addition, the elastic or Young's modulus, has theoretically been predicted and experimentally verified to equal ~ 1 TPa.[39,40] Tensile strength for individual SWNTs has been estimated to equal 22 GPa.[41] These reports correlate to strengths 10-100 times that of steel, providing additional evidence for novel SWNT materials.[39]

Although SWNTs exhibit high structural rigidity, they also have been shown to display dynamic bending abilities, allowing the deformed carbon nanotubes to elastically return to resting states. Thostenson et al, report bending angles in excess of 110°, equivalent to very high strains on the hexagonal carbon bonds.[39] Single wall carbon nanotube ribbons and fibers have also been developed. The high elastic modulus of SWNTs has been demonstrated by the ability to tie knots with bundles of SWNTs approximately 30 μm in diameter.[42] Elastic stretching appears to redistribute the hybridization of carbon atoms from sp^2 to a varying hybridization between sp^2 and sp^3, depending on the degree of strain. Others have suggested a Stone-Wales defect whereby a

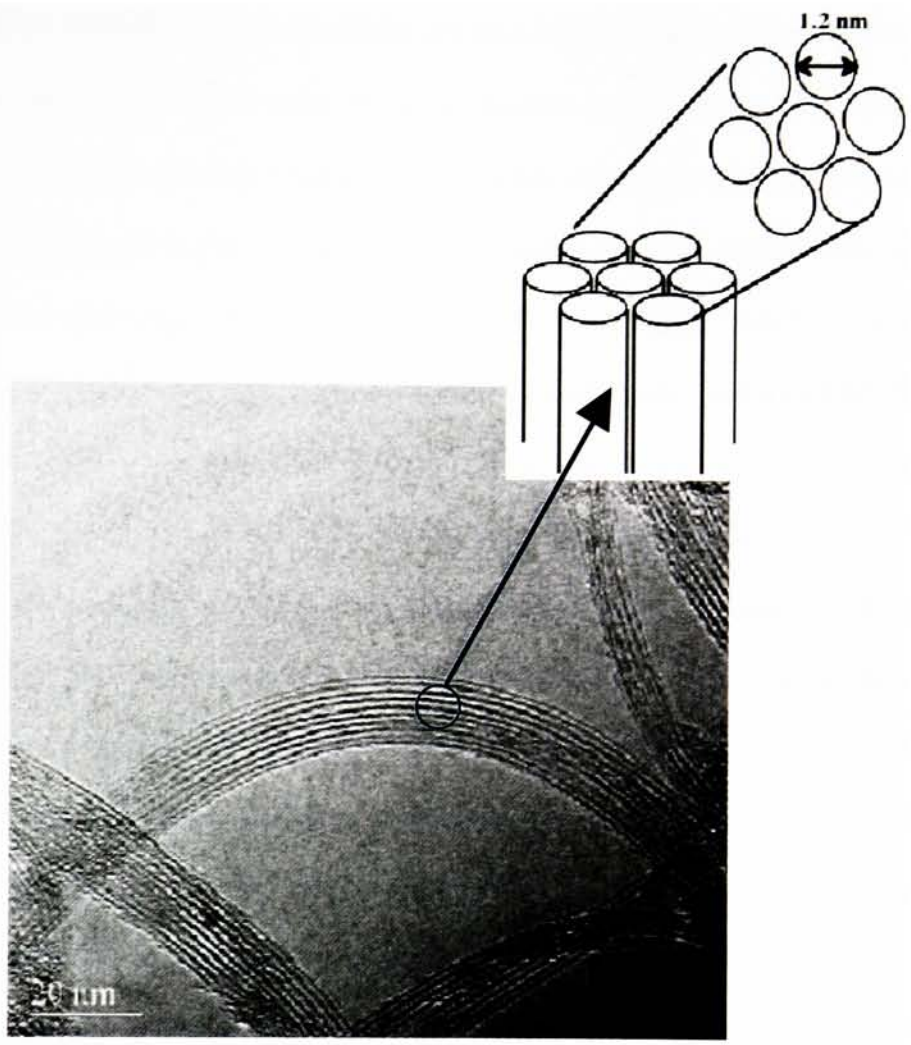

Figure 7: TEM image of purified SWNTs displaying the property of bundling. Inset shows the hexagonally close packed arrangement of the individual SWNTs that are separated by Van der Waals interations: example diameter of 1.2 nm given. (TEM performed by Mr. Kim Jones at the National Renewable Energy Laboratory, Golden, Co.)

5-7 ring system is observed when stress is applied to the SWNT, altering the diameter and chirality.[20] Applied stress can deform SWNTs in one of two manners: either kinks resulting in a buckling effect, or torsional strain. Results by Srivastava et. al., indicate a delocalization in energy from the π clouds at the site of strain, increasing chemical reactivity at that site. This nonlinear distortion may result in novel applications for SWNTs like chemisorption of atomic hydrogen,[24] or stress-induced nanotube probing.[20] Additional reports indicate that only chiral SWNTs undergo an asymmetric torsional strain compared to pristine armchair and zigzag SWNTs.[39] Consequently, variations in structure lead to significant modifications of electronic properties for SWNTs.

Many of the key applications being developed using SWNTs are a result of the unique and versatile electronic properties these materials display. The extent to which a SWNT exhibits metallic or semiconducting behavior is a direct result of the chirality associated with the individual structure. Therefore, to understand the electronic states of metallic and semiconducting SWNTs, it is pertinent to evaluate the characteristics of graphene, a 2-D structure by which carbon nanotubes theoretically derive from when curled to form a 1-D-like tube. The sp^2 hybridization of carbon atoms in the sheet displays interesting conducting properties based on the electronic band structures. The electronic state at the Fermi level is unique for graphene because the structure displays a semimetal behavior. Semimetal band structure has been described by McEuen as a crystal lattice where electrons can backscatter in the lattice like typical semiconductors, or propagate through the lattice similar to metals.[35] Graphene exhibits both properties, dependent on the angle where electrons scatter in the lattice. Consequently, SWNTs will show similar electronic properties based on the chirality, or angle of formation from the rolled up graphene sheet.[35]

1.6 Synthesis and Purification

The synthesis of SWNTs can be accomplished by several methods, each offering different distributions of purity, diameter, and chirality types. The original discovery of SWNTs was with carbon soot generated by the arc-discharge method. This method applies high voltages across two metal-doped graphitic rods in the presence of an inert atmosphere to develop a vaporized carbon plume (Figure 8).[43,44] SWNTs have also been synthesized using a laser vaporization procedure, where a source laser (such as Nd:YAG, Alexandrite, UV, IR, etc.) is applied to a metal-doped graphite target under inert atmosphere and elevated temperatures. The resultant metal-carbon vapor generates a plume which under flowing $Ar_{(g)}$, condenses outside of the furnace into a mixture of SWNTs and synthetic impurities (Figure 9).[38] However, drawbacks exist for both the arc-discharge and laser grown methods, namely the extremely elevated temperatures for carbon sources, amorphous carbon and metal impurities, and the high entanglement of SWNTs. Several of these limitations have been addressed via an alternative method, namely chemical vapor deposition (CVD) synthesis (Figure 10). Chemical vapor deposition introduces a carbon feedstock gas over a catalyst-supported substrate at moderate temperatures. This method has established a certain degree of control over helicity, diameter, and growth orientation.[45] Also, the scalability of CVD synthesis allows larger quantities of carbon nanotubes to be synthesized in a more cost-effective manner. Similar to arc and laser, current CVD techniques also display limitations on the yield, purity, and defects associated with synthesis, primarily based on the catalyst selection.[45] In an attempt to develop a synthetic procedure that could enable mass production (kg – ton) of SWNTs, Smalley et. al., proposed the HiPco process in 1999. This method employs passing $CO_{(g)}$ along with catalytic amounts of $Fe(CO)_5$ through a heated reactor chamber at optimized conditions of 1200°C and 10 atm. One significant advantage of this process is the continuous flow that allows for proposed reproducibility and scale-up potential.

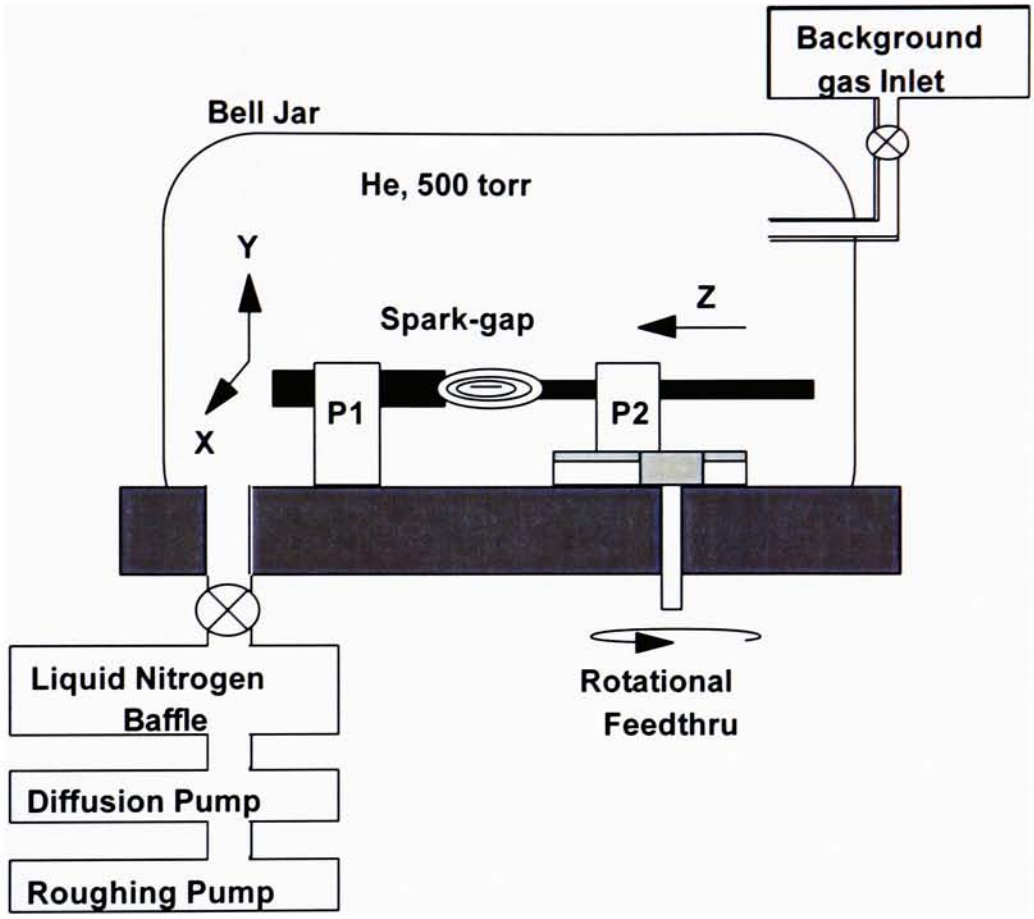

Figure 8: Representation of the arc-discharge apparatus used for synthesis of SWNTs. Application of high voltages between two carbon rods (connected at P1 and P2) at constant pressure under inert atmosphere, results in the production of a carbon plume containing SWNTs.

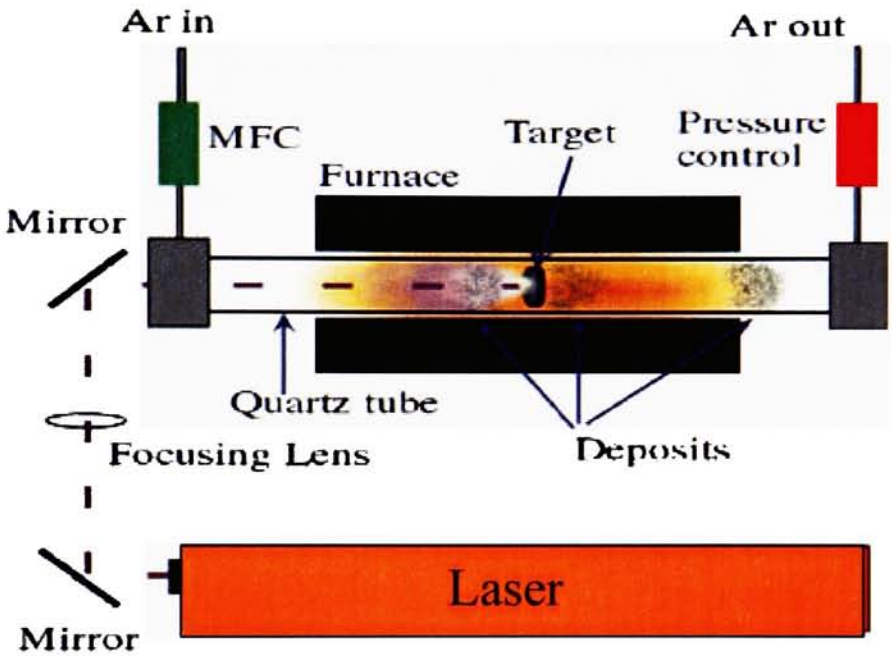

Figure 9: Representation of the pulse laser vaporization apparatus used for synthesis of SWNTs. Incident laser beam is controlled with mirrors to raster over the surface of a graphite target in a high temperature furnace at a variable pressure under inert atmosphere.

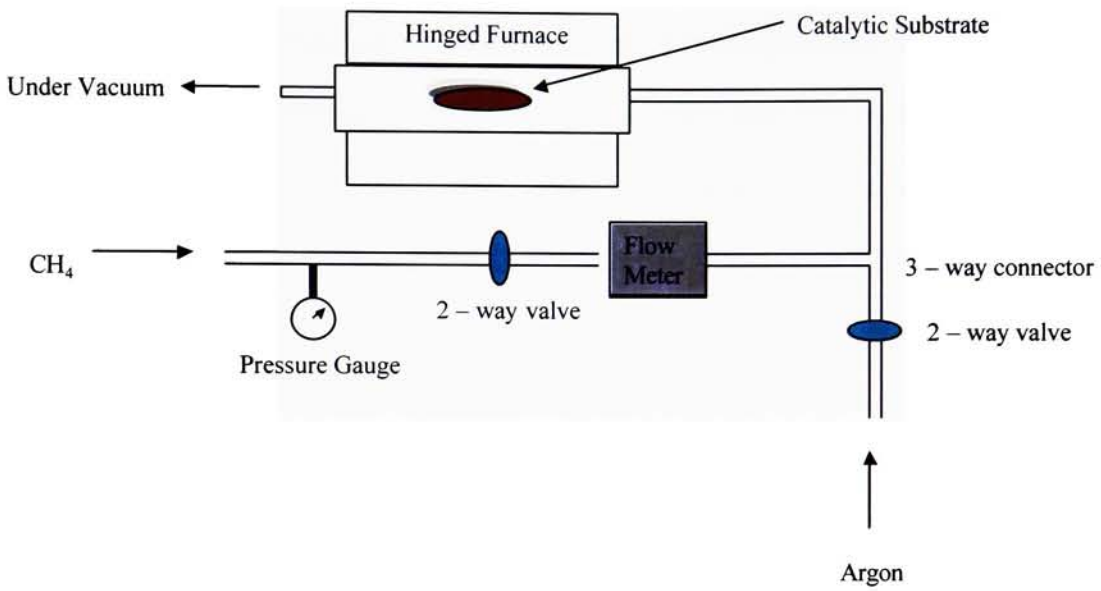

Figure 10: Representation of a chemical vapor deposition (CVD) apparatus used for synthesis of SWNTs. Introduction of a carbon feedstock gas (CH_4 is shown above) over a supported catalyst substrate at elevated temperatures results in the production of SWNTs.

While various techniques are employed for SWNT synthesis, purification has been a limiting step for many researchers to develop high purity, pristine carbon nanotubes. Many reports indicate experimental procedures for this crucial step.[31,46] Since laser-generated and commercially obtained HiPco SWNTs are of interest for this thesis project, purification techniques related to these materials will be addressed. Purification of laser-generated material has been reported by Gennett and others to produce SWNTs with purities greater than 98% w/w.[38,47] Purification of these SWNTs was achieved by a nitric acid reflux followed by oxidation in air at 550 °C. Purification of HiPco carbon nanotubes has been successful using a series of thermal oxidations with subsequent hydrochloric acid washes to remove the catalytic iron from the as-produced material.[46]

1.7 Carbon Nanotube-Polymer Composites

Another significant area of research is in the area of carbon nanotube-polymer composites. The intentions are to develop novel materials exhibiting unique electrical, thermal, optical, and mechanical properties. Evaluation of the potential uses for these nanotube-reinforced composites can highlight new technologies that will originate from carbon nanotubes. Although the preliminary development of successful composites has been achieved, current work is also directed at studying the interactions associated between carbon nanotubes and polymer matrices: the dominating property for applications in electronic devices. Several processing mechanisms have been proposed stating that the polymer backbone is capable of a promoted wrapping around the carbon nanotube to produce a uniform dispersion. The reverse-water solubilization mechanism utilizes the hydrophobic nature of carbon nanotubes by non-covalent wrapping with such polymers as poly(vinyl pyrrolidone) and poly(styrene sulfonate). These polymers promote high solubility for transfer of pristine carbon nanotubes into aqueous systems.[48] Surfactant-assisted techniques have attempted to reduce the interfacial adhesion energy between carbon nanotubes and polymers by

wetting the carbon nanotube surface with surfactants. Another proposed mechanism of dispersion shows that the polymer poly(*m*-phenylenevinylene-*co*-2,5-dioctyloxy-*p*-phenylvinylene) (PmPV), can coat SWNTs based on the helicity of the underlying carbon nanotubes. The wrapping is directly related to the interaction of the carbon nanotube and polymer, with molecular modeling displaying conformational changes in the polymer during the wrapping process. The conformation changes are proposed to correlate with $\pi-\pi$ stacking of the polymeric backbone with the hexagonal structure of the carbon nanotubes along the helical symmetries.[49] It is proposed that each polymer will interact differently with carbon nanotubes, producing a unique junction between each component. Within this junction, exists the charge transfer capability for certain electronic devices. However, any impurities in the composite can act as electron traps and distort the charge transfer process. One type being explored for photovoltaic devices is a photo induced charge transfer resulting from the junction where the photo-excited polymer, poly(3-octylthiophene), (electron donating) and carbon nanotubes (hole donating) transfer charge through the composite system.[50]

Considerable research has been devoted to developing composites that successfully transfer load requirements from the polymer backbone to the dispersed carbon nanotubes. Ideal for such applications, carbon nanotubes exhibit a large aspect ratio, which is conducive to formation of a network within the polymer matrix. The established network at high doping levels can lead to a percolation threshold, which is proportional to the aspect ratio, $\sim 10^3$ for SWNTs.[51] Since the tensile strength of carbon nanotubes has been predicted to be 10-100 times that of steel, SWNT-polymer composites could significantly enhance the strength of composite materials. Initial studies focused on MWNT-polystyrene composites for load transfer effects, concluding that 1 % w/w dispersions significantly increased the elastic modulus and break stresses of the resulting composites by ~40% and ~25%, respectively.[52] Although results are encouraging, the carbon

nanotube material used in this study was as-produced MWNTs, containing metal catalyst impurities and numerous structural defects. This preliminary work has perpetuated more in depth analyses, including the recent proposal that SWNTs present superior load transfer abilities over MWNTs, since the polymer chain is interacting directly with the outermost shell responsible for carrying the imposed load.[53] When using MWNTs, the internal shells are free to move and are only stabilized by weak Van der Waal's forces, thereby allowing eventual deterioration of composite strength. However, to develop successful composites using SWNTs, researchers have proposed the necessity to overcome the bundling effects exhibited by SWNTs. Ajayan et. al., have calculated the force required to separate SWNTs individually from the bundles. Results indicate that energetically it would be easier for a polymeric matrix to pull a SWNT from the end of the bundle, rather than normal to the bundle, overcoming the carbon nanotube's Van der Waal's interactions for the bundle. Depending on the interfacial strength between the carbon nanotube and polymer matrix, this force normal to the bundle may result in shearing of the SWNT, specifically at defective sites along the sidewall of the carbon nanotube.[54]

While load transfer composites represent one area for carbon nanotube-polymer composite applications, another significant approach utilizes the high thermal conductivity of carbon nanotubes. Since thermal transport in solid structures results from a combination of conduction by electrons and phonons, successful interaction between polymer matrices and carbon nanotubes can be used for thermal management. Since theoretical predictions for thermal conductivity in SWNTs equal 6000 W/mK,[51] the integration of SWNTs into polymer composites shows extreme potential for these applications. A recent report has shown a 125% increase in thermal conductivity for a 1% w/w as-produced SWNT–epoxy composite.[51] In addition, molecular modeling has provided certain theoretical insights to help support the observed carbon nanotube-polymer interactions. Gong et. al., have reported an increase in T_g of 25 °C, and an elastic

modulus increase of 30% for epoxy composites with 1% w/w doping of carbon nanotubes.[55] Carbon nanotube-polyethylene composites have exhibited a higher glass transition temperature, T_g, than the native polyethylene. These results have shown an increase in thermal expansion coefficients for composite systems, explained by the rigidity of dispersed carbon nanotubes with uniform phonon vibrations, preventing polymer rearrangement at higher temperatures.[56] A similar report using carbon nanotube-polystyrene composites shows enhanced interaction between polymer and carbon nanotubes due to a thermal expansion coefficient mismatch, which is proposed to increase the interlocking mechanism when composites are cooled from their melt.[57] Overall, it seems evident that integration of carbon nanotubes with polymer matrices is a complex interaction leading to potentially interesting thermal and physical properties.

While significant advances have been made in quantifying load transfer, thermal and electric effects in carbon nanotube-polymer composites using impure materials, the necessary evaluation using high purity samples will inevitably lead to more accurate results. Electrical and optical properties of carbon nanotube-polymer composites have recently been a focus of extensive research,[58] showing great promise for ultracapacitors,[59] photovoltaic devices,[50] and photosensitive applications.[60] In addition, the current molecular modeling studies have displayed several interaction mechanisms to provide an initial understanding of the roles each component plays in the composite. However, it will be through experimental modification and device development that the mechanism of interaction for each carbon nanotube-polymer composite is determined.

1.8 Carbon Nanotube-Polymer Composite Actuators

Successful integration of high purity SWNTs with a polymer matrix to develop novel devices is at the forefront of many research groups. Introduction of highly conductive SWNTs into the Nafion polymer could significantly enhance the polymer film conduction, which may be potentially sufficient for inducing actuation. Production of SWNT-Nafion composite actuators should require

homogeneous dispersion of SWNTs throughout the polymer matrix. The interaction between components may enhance debundling of purified SWNTs, thereby decreasing the percolation threshold. Actuation within these samples may occur either through faradaic or non-faradaic processes depending on the degree of dispersion and resulting actuation mechanism. If ion intercalation is able to establish an electric double layer with the carbon nanotubes, the non-faradaic process will result. However, if homogeneous dispersions are achieved, carbon nanotubes would likely be coated with polymer, allowing ion intercalation to promote actuation of the polymer component. Each of these possibilities will be evaluated upon successful actuator development. The opportunity that this technology presents is largely an improved material process, where polymer-based actuators could be made into ribbons, fibers, or sheets, entirely dependent on the application. While this blend of research contains many possibilities, the cutting edge nature provides scientific appeal and motivation for application in MEMs technologies and artificial muscle research.

2.0 Experimental

2.1 Synthesis of HiPco and Laser Single Wall Carbon Nanotubes

Single wall carbon nanotubes (SWNTs) used in this thesis project were obtained via two sources: (1) commercially obtained from Carbon Nanotechnologies, Inc.(CNI), produced by the HiPco process (h-SWNTs); (2) synthesized using pulse laser vaporization(l-SWNTs). Synthesis conditions for the HiPco process were outlined in the introduction.[30] The schematic of the pulse laser vaporization apparatus is depicted in Figure 11. The system design for the laser synthesis of single wall carbon nanotubes allows for control over multiple parameters: chamber configuration, raster pattern, furnace temperature, inert gas flow rate, chamber pressure, laser power density, and target composition. In this study, the SWNTs were synthesized in a 2.4 L single quartz tube chamber configuration, linear raster pattern over the target with a 50% overlap of a 2.5 mm laser beam spot size, furnace temperature at 1200 °C, and a flow rate of 100 sccm of $Ar_{(g)}$. The graphite (1-2 μm) target (pressed at 20,000 psi) was doped with 0.6 atomic percent each of Ni and Co. The other variables were controlled within an appropriate range to synthesize reproducible l-SWNTs, as listed by the following: chamber pressure between 300-500 mmHg, and laser power density of 100 W/cm^2.

2.2 Purification of HiPco and Laser Single Wall Carbon Nanotubes

Procedures for purifying h-SWNTs and l-SWNTs employed two different protocols, however each contained oxidative treatments with acid and air oxidations at high temperatures. The purpose of acid (whether HNO_3 or HCl) was to remove residual metal catalyst particles, while thermal oxidation at various temperatures removed the amorphous carbon impurities. The procedure for h-SWNTs was similar to the one reported by Chiang et. al.,[46] with minor modifications being the type of furnace and slight variations on sonication and thermal oxidation times. The procedure used is outlined as follows:

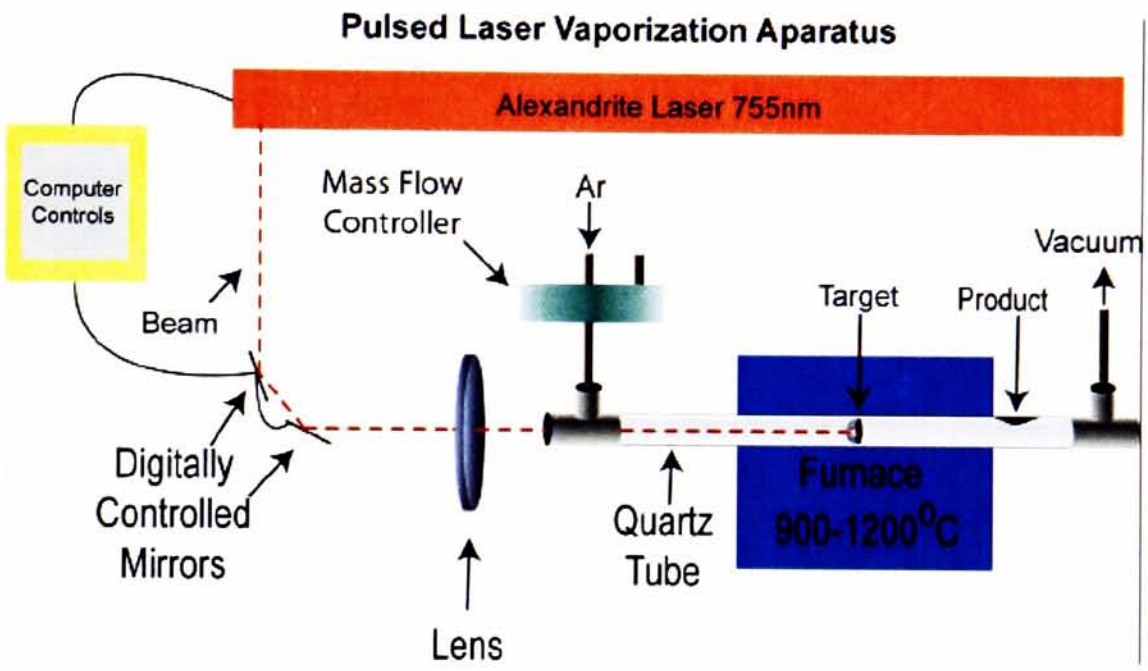

Figure 11: Representation of the pulse laser vaporization apparatus used for synthesis of l-SWNTs applied to this thesis. Incident laser beam is controlled with mirrors to raster over the surface of a Ni-Co doped-graphite target. Synthesis occurred in a 2.4 L single quartz tube chamber configuration, linear raster pattern with a 50% overlap of a 2.5 mm laser beam spot size, furnace temperature at 1200 °C, and a flow rate of 100 sccm of $Ar_{(g)}$.

Step 1: ~50-70 mg of as-received h-SWNTs were compressed on a 0.02 μm, 47 mm Anodisc filter using concentrated hydrochloric acid and placed on a $Pt_{(s)}$ boat in the muffle furnace (Thermolyne 1300) at 225°C overnight (~16 hrs) with occasional opening of door to promote air flow.

Step 2: Oxidized material was mixed with 20 mL of concentrated hydrochloric acid and placed in sonic bath (Aquasonic 75D) for 1 hour.

Step 3: Acid solution was vacuum-filtered using 0.02 μm, 47 mm Anodisc filter papers and dried at 70°C in vacuo for 1 hour.

Step 4: h-SWNT "paper" removed from Anodisc filter paper and placed in muffle furnace at 325°C for 2 hours.

Step 5: Sonication and filtration step same as (2-3)

Step 6: h-SWNT "paper" removed from Anodisc filter paper and placed in muffle furnace at 425°C for 1 hour.

Step 7: Sonication and filtration step same as (2-3)

Step 8: h-SWNT "paper" removed from Anodisc filter paper and placed in muffle furnace at 425°C for 2 hours

In comparison to the above procedure, the protocol for purifying l-SWNTs originated from the publication by Dillon et. al.,[47] where the as-produced SWNTs are refluxed in 3M nitric acid for 16 hours, followed by an air oxidation at 550°C. The only modification to the reported procedure was thermal oxidation at temperatures between 500-525°C, accounting for variations in altitude from published report. Additionally, an acid wash using concentrated hydrochloric acid after the thermal oxidation was occasionally necessary if residual metal catalyst remained. The purity for both synthetic types was always >95% w/w, the target value for purified SWNTs used in this thesis.

2.3 Characterization of Single Wall Carbon Nanotubes

Techniques used to characterize the single wall carbon nanotube material, including the polymer composites, were the following: Thermogravimetric Analysis (TGA), Scanning Electron Microscopy (SEM), optical absorption spectroscopy, and Raman spectroscopy. Each of these

methods is outlined below, as well as a brief description of the sample preparations and experimental conditions used to acquire the data.

- Thermogravimetric analysis (TGA) is a technique used to evaluate the thermal stability of materials by monitoring the change in sample mass while being ramped through a temperature range at a specified rate. The results can quantify decomposition temperatures for samples under a given set of atmospheric conditions.[61] Applied to SWNTs, the purity levels and percentage of residual metal catalyst impurities can be determined quantitatively. Demonstration of TGA analysis for SWNTs was reported by Dillon et. al., and Figure 12 shows the overlay for the purification process.[47] The decomposition transition labeled (A) corresponds to the amorphous carbon impurities, which decompose at lower temperatures compared to the (B) SWNTs. In addition, qualitative analysis pertaining to the percentage of SWNTs in the as-produced material can be evaluated.[47] The TGA instrument utilized for this thesis project was a TA Instruments Model 2950. Samples were applied to a platinum pan in quantities between 0.3-1.0 mg and ramped at 5°C/min from room temperature up to 950°C under air at a gas flow rate of 50 cm^3/min and $N_{2(g)}$ purge at a gas flow rate of 40 cm^3/min.
- Scanning Electron Microscopy (SEM) is a technique used to evaluate the surface characteristics of a sample by detecting the electron scatter from the sample surface.[61] The microscopy analysis provides a sample-limiting, qualitative understanding of the sample contents for imaged regions. When evaluating SWNTs, the analysis provides information related to purity, including amorphous carbon coatings and metal catalyst content. Additionally, SEM can provide an understanding of SWNT bundling effects, specifically the bundle diameters.[46] Images generated for as-produced SWNTs, purified SWNTs, and SWNT-doped polymer composites can compare the effects each

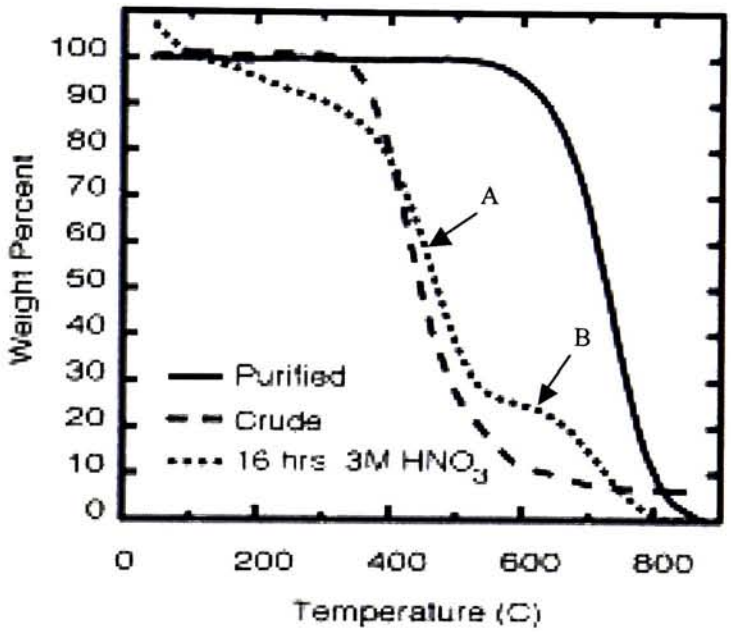

Figure 12: Thermogram depicting the changes in weight percent of SWNTs over a temperature range during thermogravimetric analysis. Transition (A) represents the amorphous carbon impurities, and (B) represents the SWNTS for the 16 hrs. 3M HNO_3 sample.

experimental modification has on the bundling effects of the SWNT material. The SEM instrument used was a Hitachi S-900. Samples were prepared by applying SWNT material directly to carbon tape, or by suspending SWNTs in acetone and then placing a drop of solution on a TEM grid, which was applied to carbon tape or applied directly to sample stub using silver paint. The instrument operated at an accelerating voltage of 2 kV and magnifications ranged from 5- 100 kX, with good picture quality.

- Optical absorption spectroscopy is a common technique for evaluating the effects of electromagnetic radiation on a sample in the UV-Vis-NIR region (120-2500 nm), specifically the electronic transitions and optical bandgaps.[61] Single wall carbon nanotubes have characteristic absorption peaks corresponding to changes in the electronic density of states, related to Van Hove singularities: ranging from 1200-1900 nm for the 1st singularity, 800-1100 nm for the 2nd singularity, and 500-700 nm for the 3^{d} singularity under typical arc or laser synthesis conditions for SWNTs.[62] Modifications of these absorption peaks can be used to evaluate dopant effects on the electronic transitions of SWNTs as well as quantifying the diameter distributions of the SWNT samples.[63] The UV-Vis-NIR instrument used was a Perkin-Elmer Lambda 900. SWNT samples were typically prepared by spraying quartz plates with suspended material in acetone (~1 mg/10 mL), The suspensions were prepared by sonication for 30 minutes and sprayed via an Anthem No.155-7 sprayer under 20 psi $N_{2(g)}$, over the surface of the quartz plate. Homogeneous coverage was achieved when care was taken to dispense the sprayed solution at appropriate rates. Polymeric samples for UV-Vis-NIR analysis were either solution cast on quartz plates or thin films prepared for scans if SWNT concentrations in the polymer composites were low enough to cause transparency. The instrument scanned over a wavelength range of 200-2500 nm at a data interval of 1 nm. In the NIR range,

the instrument scan speed was 375 nm/minute, integration time of 0.16 seconds, slit equal to 1 nm, and gain set at 1. For the UV-Vis region, the scan speed was 375 nm/minute, integration time 0.12 seconds, slit equal to 4.0 nm, and gain set at 1.

Resonant Raman spectroscopy is a technique used to monitor symmetric vibrations of a sample at an excitation wavelength corresponding to an absorption peak. During Raman excitation, the electrons are promoted to an excited state and immediately relaxed to a vibrational level at the ground state. This analysis uses a tunable laser that can identify the sample's maximum absorption wavelengths over a range by showing an increase in the Raman intensity for each characteristic vibrational transition.[61] Specifically, Raman spectroscopy has been shown to evaluate the diameter distributions for semiconducting and metallic SWNTs due to resonant enhancement of the radial breathing mode, dependent on the excitation wavelength.[64] For the series of experiments performed in this project, 488 nm excitation corresponds to semiconducting SWNTs, while 633 nm excitation is for metallic SWNTs.[64] The Raman instrument used was a Jobin-Yvon Super LabRam Model 011; SWNT samples were analyzed using an MSPLAN-100 objective with 488 nm excitation from a 649 mW argon ion laser and 633 nm excitation from a 20 mW HeNe laser. The scan range was 150 – 3000 cm^{-1} and the resolution of the 633 nm excitation Raman data was 2.94 cm^{-1} at 150 cm^{-1} Raman shift and 1.96 cm^{-1} at 3000 cm^{-1} Raman shift. During 488 nm excitation, the resolution was 4.96 cm^{-1} at 150 cm^{-1} Raman shift and 3.67 cm^{-1} at 3000 cm^{-1} Raman shift.

2.4 Four-Point Conductivity of SWNT "Paper" and Polymer Composites

Measurements were conducted on SWNT "buckeypapers" and polymer composites using a 4-point wafer probe to determine volume resistance that was converted to volume conductivity for the samples. The instrument was a Keithley programmable source unit with multimeter, set at

a voltage limit of 10.0 V and a continuous source current ranging from 1.0000 E-02 – 1.0000 E-03 Amps. Instrument values allowed for computation of an average voltage that was used to determine the resistivity (ρ) upon correction for probe spacing and sample volume. The conductivity (σ) was then calculated by taking the reciprocal of ρ. These values represent the volume conductivity for the SWNT samples and composite films, within experimental error.

2.5 Procedure for Preparing Single Wall Carbon Nanotube-Polymer Composites

Single wall carbon nanotube-polymer composites were prepared by addition of appropriate values of carbon nanotubes to a predetermined volume of polymer. The equation **(1)** used to calculate percent by weight of SWNTs in the polymer is the following:

Equation 1:

$$\text{Percent by weight} = \{\text{mass SWNTs} / [(\text{polymer density} * \text{polymer volume} * \text{percent by weight polymer}) + \text{mass SWNTs}]\} * 100$$

The composite solutions (mixture of appropriate mass of SWNTs and volume of polymer solution) were first homogenized for five 10-minute intervals using an IKA Ultra Turrax T25 mixer at a speed setting of 5 for 20 minutes, until a highly homogeneous solution resulted. The solutions were then exposed to high shear stirring at room temperature for 72 hours in a 20 mL. After 72 hours, the solutions were centrifuged to remove any non-dispersed materials. After centrifugation, the mass of any residue was determined and the percent by weight was adjusted accordingly. Using traditional solution-casting techniques, thin film membranes of ~25 μm thickness were cast onto a Bytac® substrate. After stabilizing for 24 hours in air, the membranes were dried *in-vacuo* (100 mtorr) at 70°C for 30 minutes. The resultant membranes were then easily removed from the casting plate.

2.6 Preparation of Platinized SWNT-Nafion Composites

Reproducible electrical contacts to the Nafion composite membrane were achieved by utilizing the previously reported chemical reduction of platinum ions on the surface of the Nafion membrane.[65] The platinization of the composite films was achieved by first immersing the composite membrane (~10 mm x 40 mm) into 20 mL 4mM tetraamine $Pt(II)Cl_2$ solution for 45 minutes.[65] The membrane was removed, washed and re-immersed into a 20 mL 0.1 M $NaBH_4$ 3:1 (distilled water:methanol) solution to reduce the Pt (II) to Pt (0) for 1 hour. The anionic nature of the composite membrane and the kinetic control of the experiment limited the depth of penetration of the borohydride anion. After chemical reduction of Pt(II) to Pt(0), the membrane was thrice immersed for 1 hour in 20 mL of 0.3 M $HClO_4$ acid solution. These washes removed residual Pt (II) ions and reconverted the Nafion membrane to the protonated form. The platinized films were dried at 70°C *in-vacuo* for 1 hour.

2.7 Fabrication of Bimorph Cantilever Actuators

Bimorph cantilever actuators were prepared similarly to those by Baughman et. al.,[5] placing two electrodes on each side of an insulating substrate. Strips of the platinized SWNT-Nafion composites were cut in dimensions of 5 mm x 25 mm and applied to each side of a polyimide insulator using GE Varnish. The composite films dried for 4-6 hours on the polyimide substrate at room temperature. Platinum wire electrical leads were placed at one end of the polyimide insulator with a Teflon clamp (VWR) pressing contacts between electrodes and wires. The clamp's joint was sealed using GE Silicone II and the actuator was allowed to cure overnight at room temperature. During deflection analysis, a reflective mirror was necessary on the tip of the actuator. A thermal deposition of aluminum onto Kapton tape provided the reflective surface and samples were cut into dimensions of 3.5 mm x 5 mm and applied to the actuator tip. The overall SWNT-Nafion composite film electrode design and setup is depicted in Figure 13.

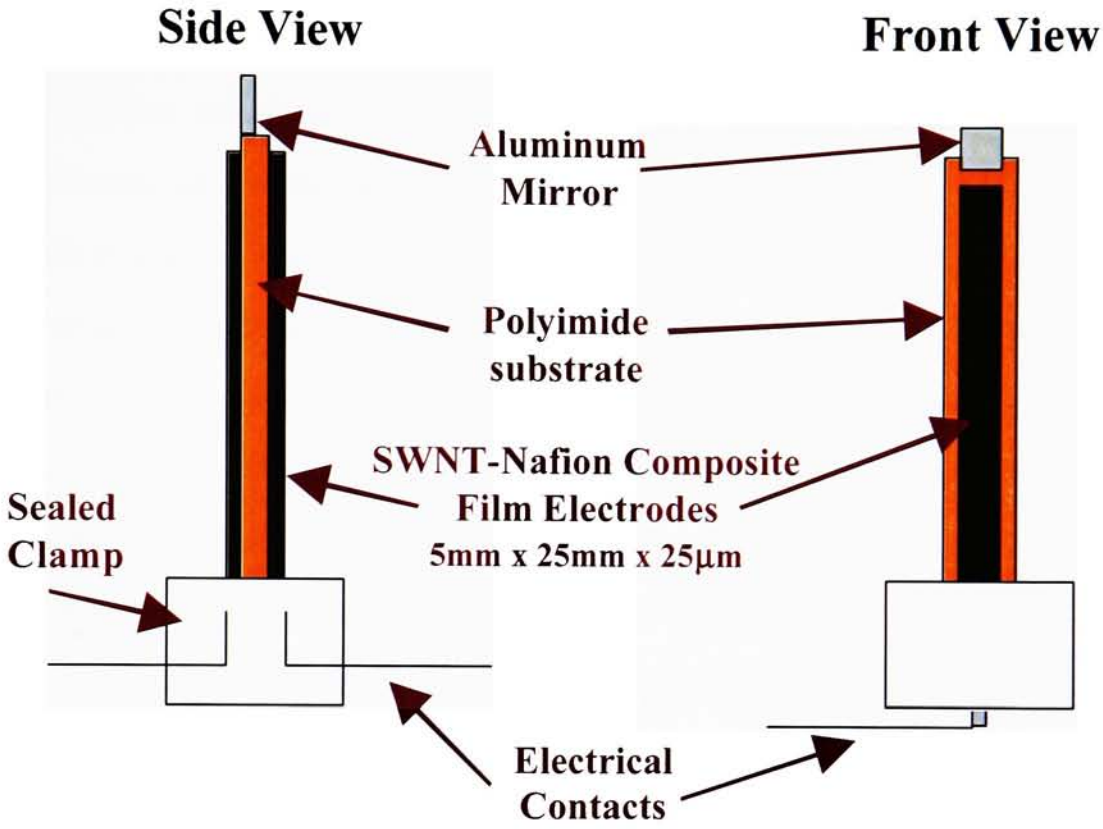

Figure 13: Schematic for the fabrication of bimorph cantilever actuators. SWNT-Nafion Composite thin film electrodes were applied to each side of a polyimide substrate; electrical contacts were applied with a sealed clamp.

2.8 Actuator Deflection Analysis using Optical Lever Apparatus

Evaluation of each actuator was performed using a laser deflection apparatus employing an optical lever to ascertain cantilever actuator tip deflections. The bimorph cantilever actuator as described above was inserted into a 1 M $LiCl_{(aq)}$ solution with the electrolyte solution level completely submerging the platinized SWNT-Nafion electrodes, and the mirror protruding vertically out of solution for deflection analysis. The incident laser beam, a 0.95 mW Helium – Neon laser, was focused onto the actuator mirror surface. The reflected beam was monitored using a data collection board. The actuator was electrically stimulated by a Keithley 236 Source Measurement Unit under the following conditions: excitation step voltages ranging from ± 0.025 V to ± 2.0 V and observable cycling frequencies from 1 to 50 Hz. The setup for the actuator deflection analysis is depicted in Figure 14. Measurements were conducted immediately upon placing the actuator in the electrolyte solution.

Quantification of the bimorph cantilever actuator tip was achieved through integration of optical lever theory. As represented in Figure 14, and using small-angle approximations for the deflections, geometry enables the following expression to be derived:

Equation 2:

$$d = D^* L/2B$$

The variables are as follows: d - bimorph cantilever actuator tip deflection; D - projected displacement; L – length of cantilever arm measured from center of mirror to the clamp; and B – distance between the actuator and data collection board. The calculated experimental tolerance for these measurements is ± 5 μm at a distance B, equal to 1 m.

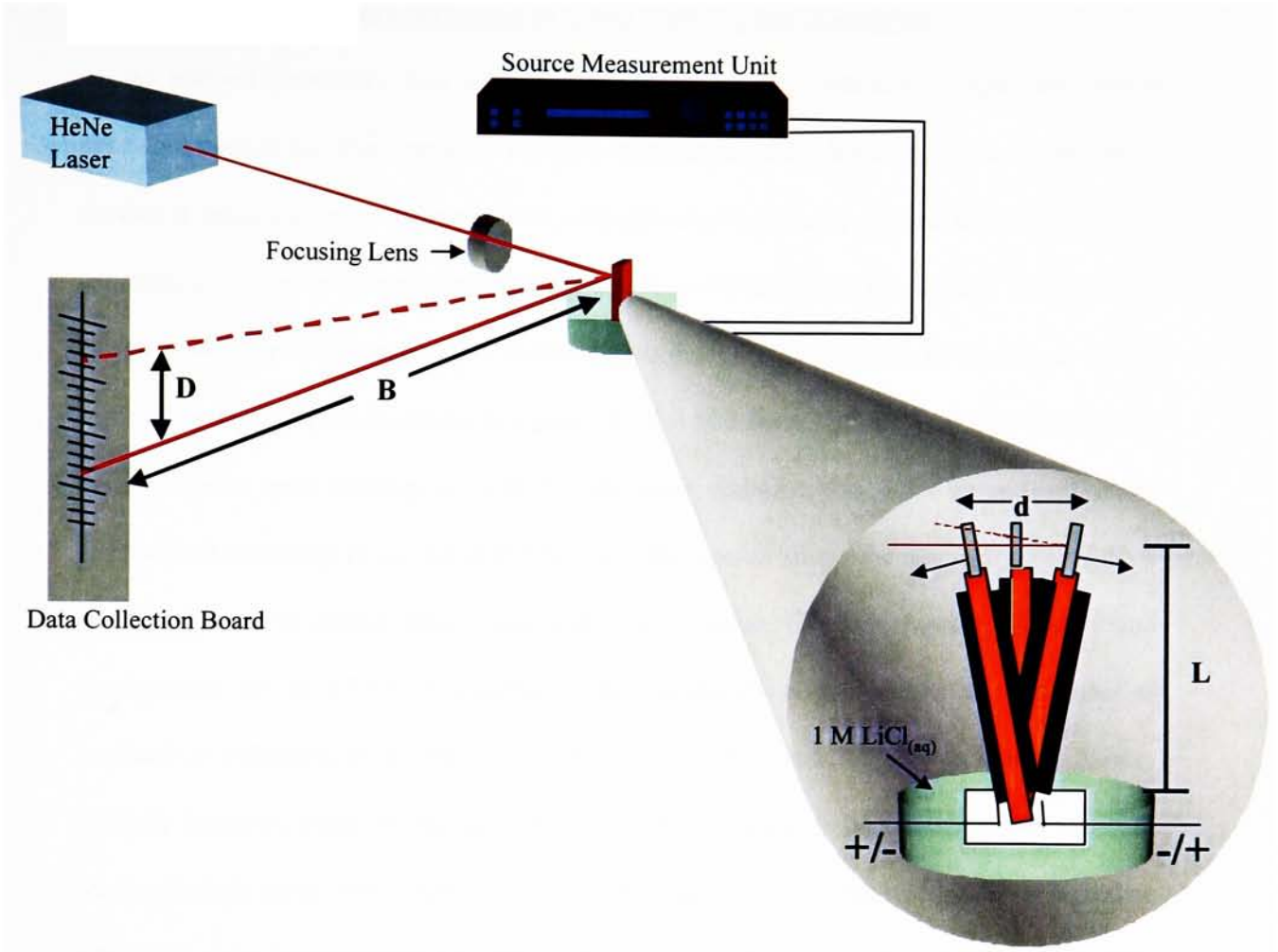

Figure 14: Diagram of optical lever analysis for acquisition of bimorph cantilever actuator displacement data. Incident Helium-Neon laser beam is focused on the aluminum mirror at the tip of the actuator (as per Figure 11), and projected to a data collection board for analysis. Variables presented for satisfying **Equation 2: d = D* L/2B,** where the variables are the following: d – bimorph cantilever actuator tip deflection; D – projected displacement; L – length of cantilever arm measured from center of aluminum mirror to the top of clamp; and B – distance between actuator tip and data collection board.

3.0 Results and Discussion

3.1 Purification and Characterization of Single Wall Carbon Nanotubes

As outlined previously, two methods were employed for synthesizing single wall carbon nanotubes used in this thesis project. For both synthetic processes however, it was imperative to develop a successful, reproducible method of purification to remove residual metal catalyst and amorphous carbonaceous impurities before proceeding with composite preparation. An overview of the h-SWNT purification process, modified from the reported procedure by Chiang et. al.,[46] is depicted by the TGA results shown in Figure 15. The as-received h-SWNTs display a prominent metal oxidation peak initiating at ~150 °C, and onset decomposition following at 325°C, with residue from remaining Fe_2O_3 being 27.5% w/w. The overlay shows the progressive removal of iron metal catalyst residue from concentrated HCl washes, and higher onset decomposition temperatures for the h-SWNTs' transition. This reproducible method allowed the conversion of hundreds of milligrams of as-received h-SWNTs into purified material. The purification process typically produced yields averaging ~10% w/w SWNT content from the as-received material. Moreover, high purity, >95% w/w, h-SWNTs following the aforementioned purification procedure exhibit an onset decomposition temperature from TGA of 465°C, and the residue is 3.3% w/w (Figure 16). Qualitative evaluation of the as-received and purified h-SWNTs was accomplished by SEM analysis. Figure 17a illustrates the surface characteristics of a random sample taken from Lot Hpr 86- the as-received material from CNI. The amorphous coating and bundling is apparent, but it is extremely difficult to assess what degree of impurities is present with this technique. Reported TEM images[46] illustrate the metal catalyst impurities present in this material, specifically Fe particles are embedded in coated SWNT bundles. Therefore, the purification procedure requires the thermal oxidation with subsequent acid washes to remove the amorphous coatings and embedded metal catalyst impurities.

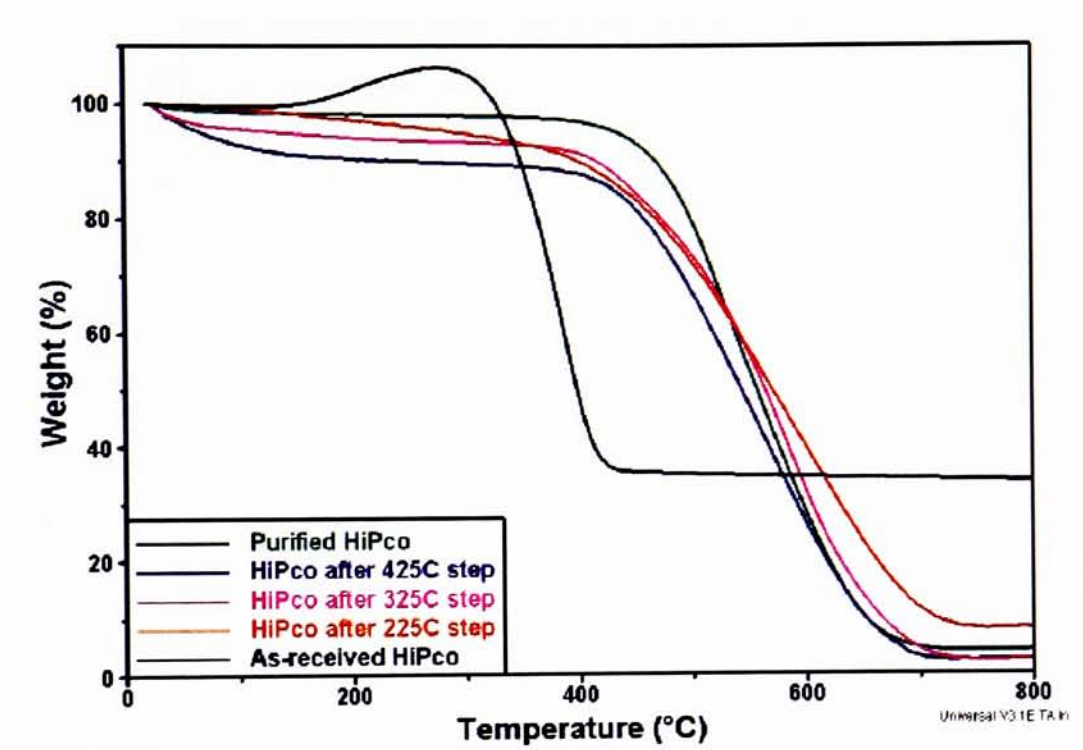

Figure 15: TGA overlay representative of the purification process used for h-SWNTs. Data is shown from each step during the purification process after thermal oxidation at 225°C, 325°C, 425°C, and anneal at 425°C.

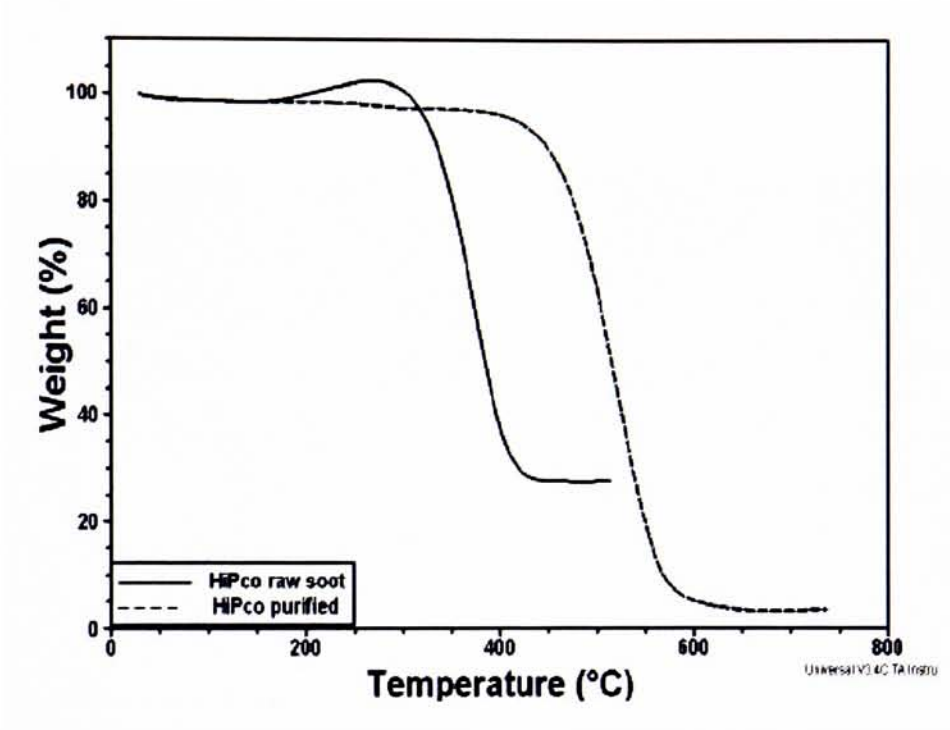

Figure 16: TGA overlay comparison between as-received h-SWNTs and high purity, >95% w/w h-SWNTs.

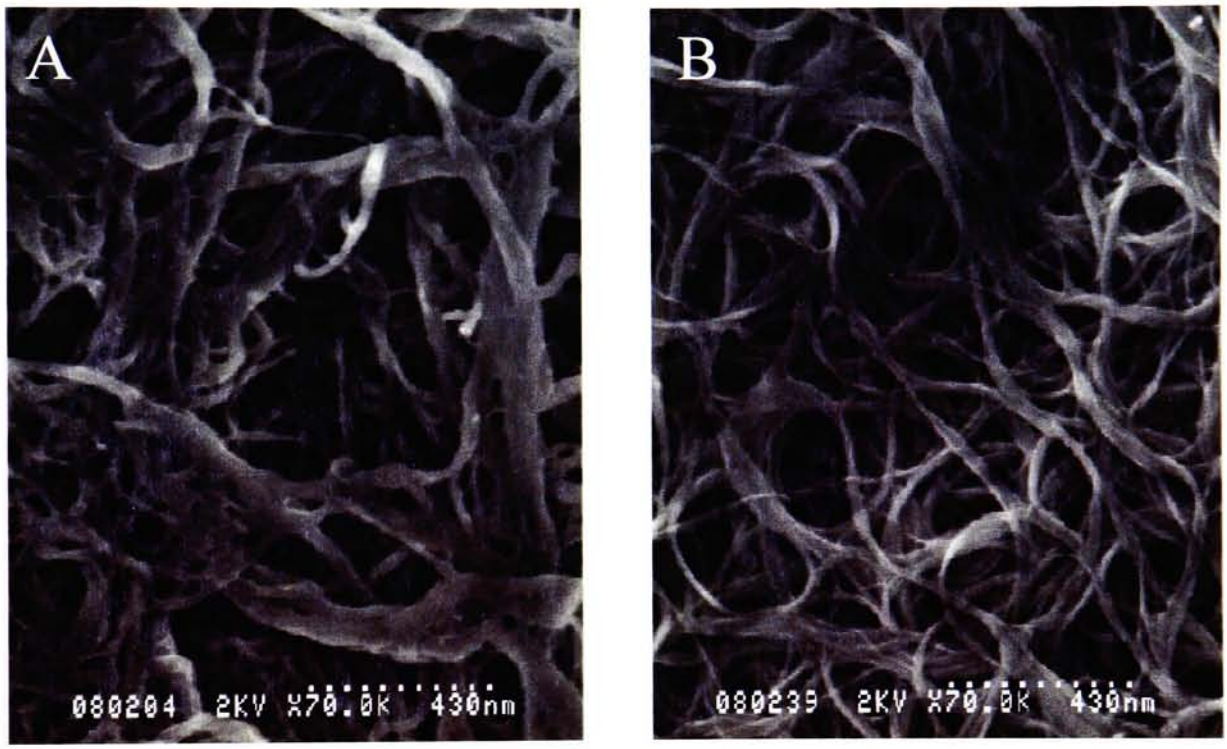

Figure 17: SEM images of (A) as-received h-SWNTs, and (B) purified, >95% w/w, h-SWNTs. Magnification is 70,000x for both images.

Single wall carbon nanotubes produced via the pulse laser vaporization technique exhibit slightly different purity and thermal oxidation properties than those for h-SWNTs. The typical synthesis conditions outlined previously yielded as-produced l-SWNTs at a rate of ~100 mg/hr, with l-SWNT content ranging from 10-40% w/w as evidenced from TGA. Purification of these materials was more straightforward than h-SWNTs, in that less steps and a shorter time period were required to achieve equivalent purities. A representative TGA overlay for the as-produced and >95% w/w, purified l-SWNTs is displayed in Figure 18. Compared to h-SWNTs, two differences are apparent for l-SWNTs, namely the lack of a metal oxide transition and separation of the amorphous carbon (region A) and SWNT decomposition transitions (region B).[47] Another important observation is the higher onset decomposition temperature for both as-produced and purified l-SWNTs compared to h-SWNTs. As-produced l-SWNTs exhibit an onset decomposition temperature of ~315 °C, and the residue is 14.6% w/w. The purified l-SWNTs, >95% w/w, have an onset decomposition temperature of 625 °C, and the residue is 3.8% w/w. Realizing however, variations in laser synthesis can lead to controlled modification of as-produced SWNT properties, thereby altering the metal catalyst impurity and amorphous carbon contents. SEM images for the as-produced and purified l-SWNTs are shown in Figure 19. Since the report by Dillon et. al.,[47] specifically states that any variation in synthesis which leads to metal encapsulation may impede the success of the reported purification process. At times, the purification procedure was modified with an HCl wash in the sonic bath to remove any previously encapsulated metal impurities from synthesis. However, it is shown that the degree of amorphous coatings observed for h-SWNTs is not present with the l-SWNTs, but bundling is still apparent. Although these variations are initially present between the as-produced h-SWNTs and l-SWNTs, reproducible purification procedures unique to each material have been demonstrated and qualitative evaluation of the purified SWNTs are quite similar, shown by SEM in Figures 17b and 19b, respectively.

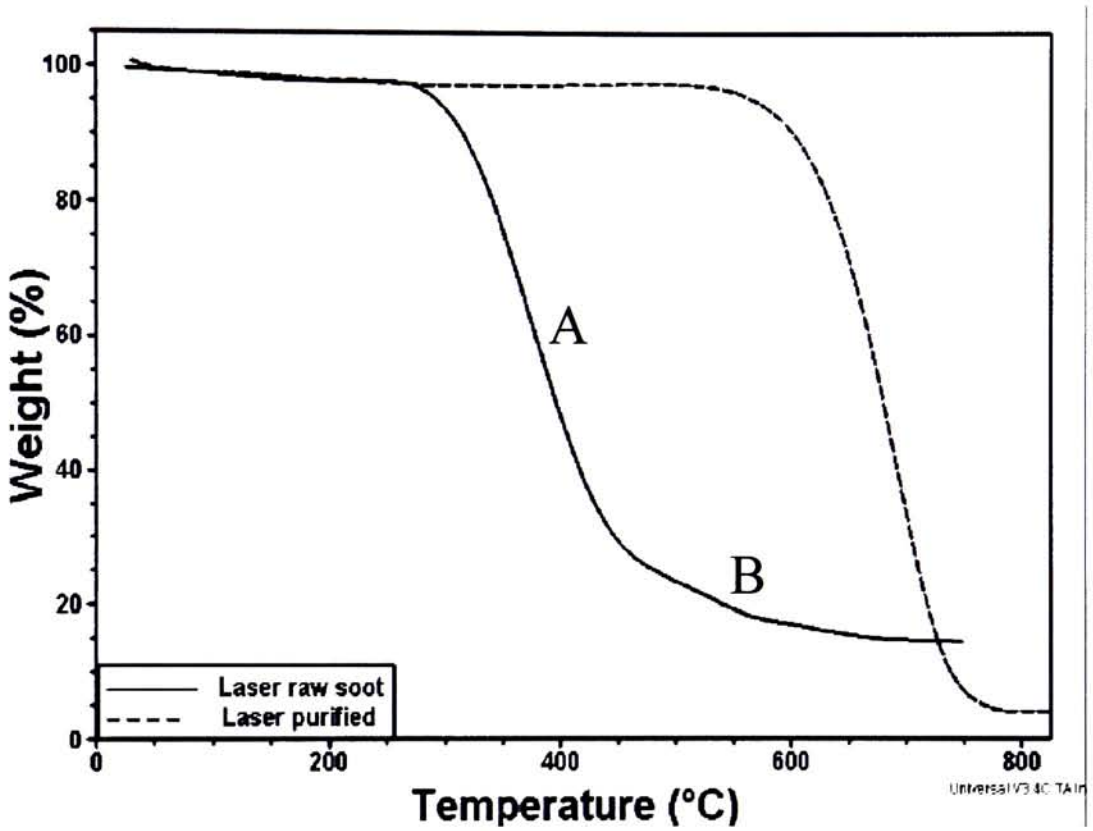

Figure 18: TGA overlay comparison between as-produced l-SWNTs and high purity, >95% w/w l-SWNTs. The separation in transitions between (A) amorphous carbon, and (B) SWNTs is identified above.

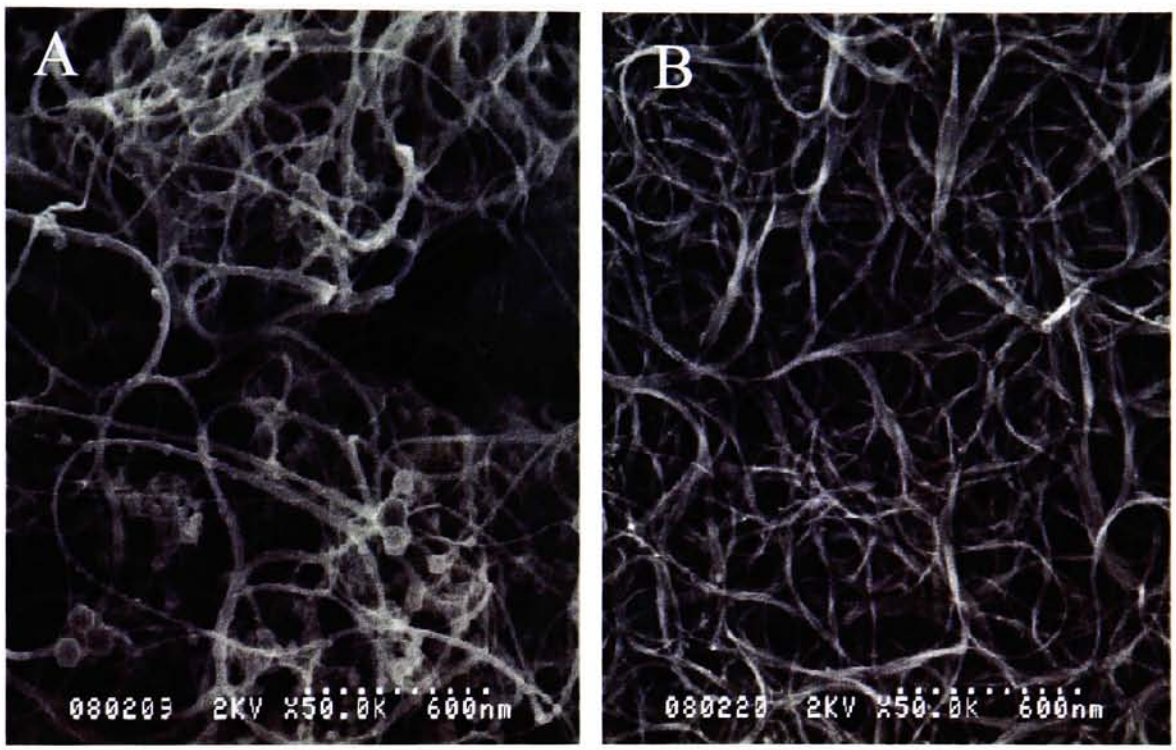

Figure 19: SEM images of (A) as-produced l-SWNTs, and (B) purified, >95% w/w, l-SWNTs. Magnification is 50,000x for both images.

Evaluation of the surface conductivity for the purified l-SWNT "papers" was performed using 4-point probe measurements. An initial evaluation of the approximate conductivities for these materials was conducted. Variations in synthesis have been shown to alter the ratio of metallic:semiconducting for the as-produced l-SWNTs.[66] Displayed in **Table I** are the synthesis dates and average conductivities (S/cm) for a series of l-SWNT "buckeypapers." The overall average value for 95% confidence was 106 ± 45 S/cm, which is two orders of magnitude less than theoretical predictions for the maximum conductivity of a metallic SWNT.[67] Similar experiments with h-SWNTs were not conducted due to the purification procedure, which produced purified material in quantities not applicable for resistivity measurements.

Table I: Four-Point Probe Conductivity Measurements for l-SWNTs

Synthesis Date	**Average Conductivity (S/cm)**
3/16/01	124.6
3/19/01	55.6
3/20/01	219.2
3/27/01	42.0
4/5/01	29.4
5/21/01	129.1
7/13/01	97.6
7/14/01	141.9
7/16/01	122.1
Average (95% confidence)	**106 ± 45**

Characterization of SWNTs for diameter distributions, relative ratios of metallic:semiconductor SWNTs, and electronic effects has been determined by spectroscopy, namely optical absorption and Raman spectroscopy. Previous work has shown the relationship between the absorption peak in the near-infrared region corresponding to the density of states responsible for the 1st Van Hove singularity in semiconducting SWNTs.[68] This absorption peak is typically centered between 1400-1800 nm, allowing the diameter range of semiconducting SWNTs present in the sample to be calculated, shown by the following equation:

Equation 3:

$$d=(8.041 \times 10^{-4})\lambda$$

The λ_{max} of the absorption peak (nm) is used to calculate the appropriate mean SWNT diameter distribution (nm).[68] Evident from Figure 20 for h-SWNTs, there is a significant difference in diameter distribution in as-produced and purified h-SWNTs. From the purification, an observed reduction in slope of the as-produced material displays the peak related to the 2nd Van Hove singularity. Other transitions at higher energies are also shown, which correspond to metallic transitions.[68] Similarly, in Figure 21 the optical absorption spectrum is shown comparing as-produced l-SWNTs to purified l-SWNTs. Interestingly, the 3rd Van Hove singularity attributed to metallic SWNTs is more prominent. Although the h-SWNTs exhibit a considerable shift in the 1st Van Hove singularity, the l-SWNTs display relatively no shift. This result may be attributed either to digestion of smaller diameter SWNTs during the h-SWNT purification process or bundling effects which may alter the absorption properties. While relative comparisons between peak heights and shifts in λ_{max} maybe important, the glaring difference between h-SWNTs and l-SWNTs is the diameter distribution effects. Figure 22 represents an overlay of the optical absorption spectra for purified h-SWNTs and l-SWNTs. Corresponding to the diameter relationship depicted in the figure from the 1st Van Hove singularity, the diameter distribution for h-SWNTs ranges between 0.8 – 1.2 nm, and for l-SWNTs between 1.1 – 1.5 nm. These values are important since the aspect ratios of the SWNTs will be directly related to the diameter distribution, potentially altering the percolation threshold for each SWNT type upon dispersion into polymer matrices. Another interesting observation with Figure 22 is the relative peak ratios from the 1st to 2nd Van Hove singularities, for h-SWNTs and l-SWNTs. Clearly the intensity ratio of the l-SWNTs (3.0) is higher than the h-SWNTs (2.5), potentially indicating certain impurity doping effects which have been previously shown to quench the 1st Van Hove intensity.[62,63]

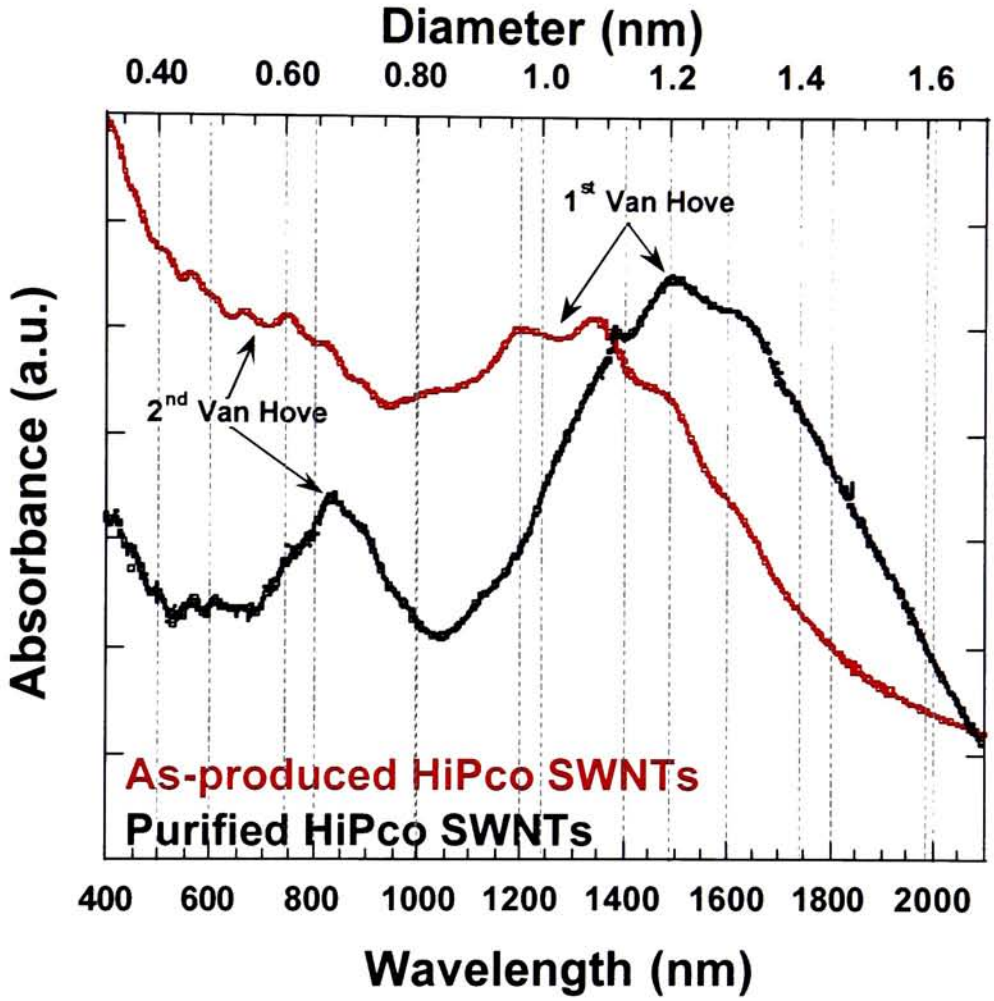

Figure 20: Optical Absorption overlay for as-received h-SWNTs and purified, >95% w/w h-SWNTs. The absorption peaks are labeled for the 1st and 2nd Van Hove singularities of the semiconducting h-SWNTs. Corresponding diameters to the semiconducting SWNTs from the 1st Van Hove absorption peak are labeled on upper x-axis.

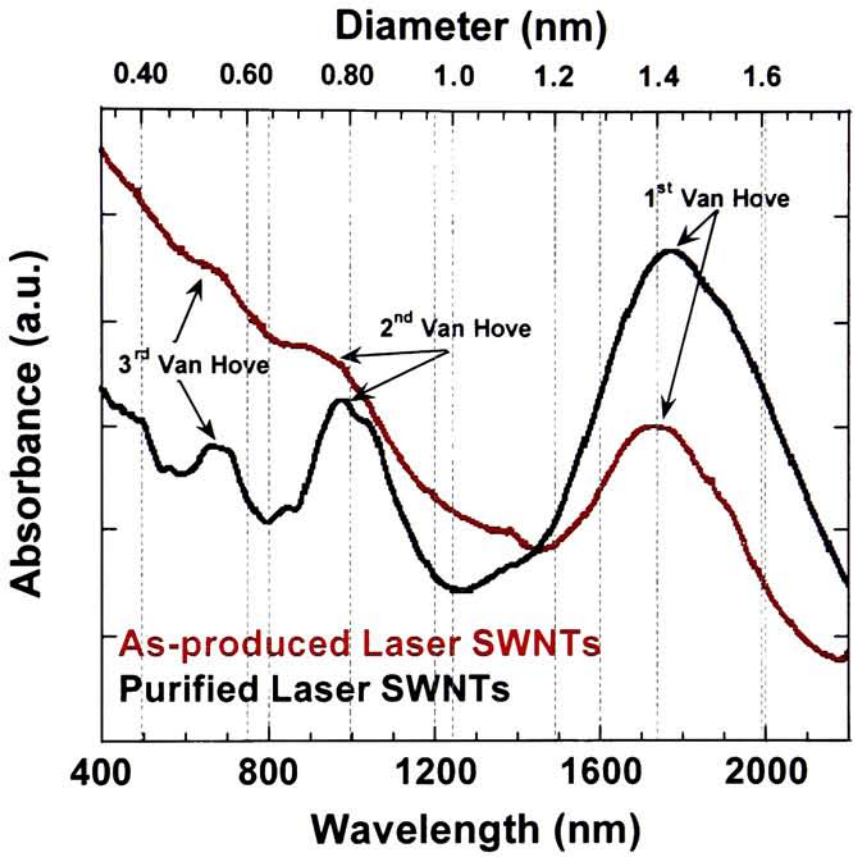

Figure 21: Optical Absorption overlay for as-produced l-SWNTs and purified, >95% w/w l-SWNTs. The absorption peaks are labeled for the 1st and 2nd Van Hove singularities of the semiconducting h-SWNTs and the 3rd Van Hove singularity correlating to the metallic l-SWNTs. Corresponding diameters to the semiconducting SWNTs from the 1st Van Hove absorption peak are labeled on upper x-axis.

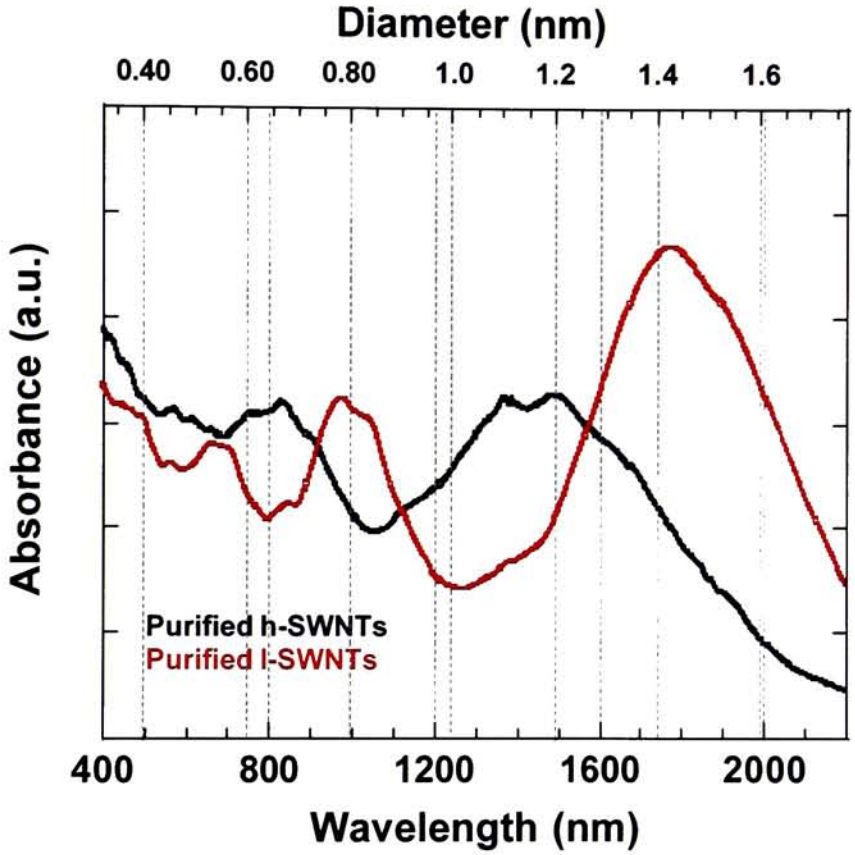

Figure 22: Optical Absorption overlay for purified, >95% w/w, h-SWNTs, and purified l-SWNTs. Relationship between the absorption wavelength for the peak corresponding to the 1st Van Hove singularity and diameter distribution of the SWNTs is shown. Relative peak ratios between 1st and 2nd Van Hove absorption peaks for purified h-SWNTs and purified l-SWNTs are 2.5, and 3.0, respectively.

Confirmation of the diameter distributions observed by optical absorption spectroscopy was achieved through evaluation of the radial breathing mode from Raman spectroscopy.[64] Figure 23 displays the Raman spectra associated with excitation at 488 nm, which results in resonant enhancement of semiconducting SWNTs. Dresselhaus et. al., have reported the relationship between Raman shift and SWNT diameter, evident by the following equation:

Equation 4:

$$\omega_{RBM} = 223\ cm^{-1}/d_t$$

The Raman shift, ω_{RBM} (cm^{-1}), is used to calculate the diameter of the SWNTs, d_t (nm).[64] Results indicate a diameter distribution for h-SWNTs of 1.0 - 1.25 nm, coinciding with the distribution from UV-Visible-NIR spectroscopy. Likewise, the diameter distribution for the l-SWNTs is between 1.25 - 1.45 nm, also in the range from UV-Visible-NIR spectroscopic results. For the metallic SWNTs, resonant enhancement of the radial breathing mode occurs at excitations of 633 nm, shown in Figure 24. The diameter distribution for h-SWNTs is slightly different, with the range consisting of 0.8 - 1.25 nm. However, for l-SWNTs the diameter distribution range is 1.15 - 1.45 nm. Overall, optical absorption spectroscopy coupled with Raman spectroscopy has evaluated the SWNTs used in this project and determined the diameter distribution ranges to be the following: 0.8 - 1.25 for h-SWNTs and 1.15 - 1.45 for l-SWNTs.

3.2 SWNT-Polymer Composites

Selected polymer matrices were investigated for composite dispersions with h-SWNTs and l-SWNTs at varying percents by weight. Development of practical applications for SWNT-polymer composites is dependent on homogeneous dispersions, whether for load transfer from polymer matrix to SWNTs, or percolation networks by the SWNTs responsible for electrically conductive pathways. An initial study of polymers and surfactant molecules was conducted to determine the materials suited for successful dispersion of SWNTs. The structures in Figure 25 represented by

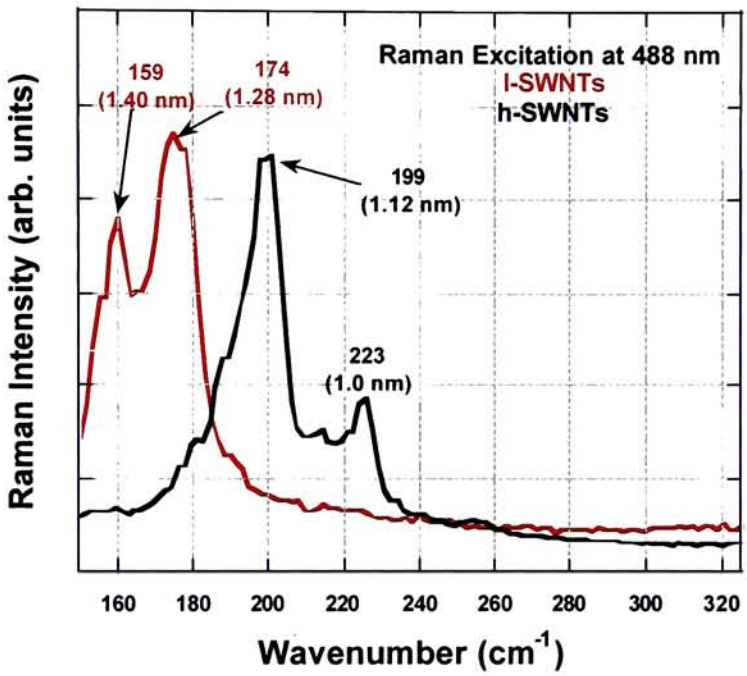

Figure 23: Overlay of raman spectroscopic data for h-SWNTs and l-SWNTs. Raman excitation at 488 nm, corresponds to resonant enhancement of the semiconducting SWNTs. Raman shifts shown in the radial breathing mode correlate to SWNT diameter distributions (nm) from the following equation: $\omega_{RBM} = 223\ cm^{-1}/d_t$

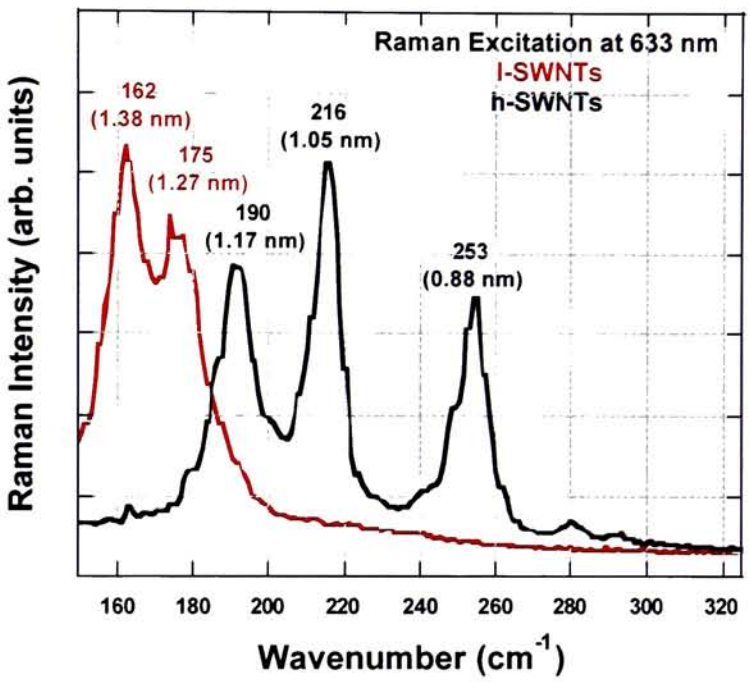

Figure 24: Overlay of raman spectroscopic data for h-SWNTs and l-SWNTs. Raman excitation at 633 nm, corresponds to resonant enhancement of the metallic SWNTs. Raman shifts shown in the radial breathing mode correlate to SWNT diameter distributions (nm) from the following equation: $\omega_{RBM} = 223\ cm^{-1}/d_t$

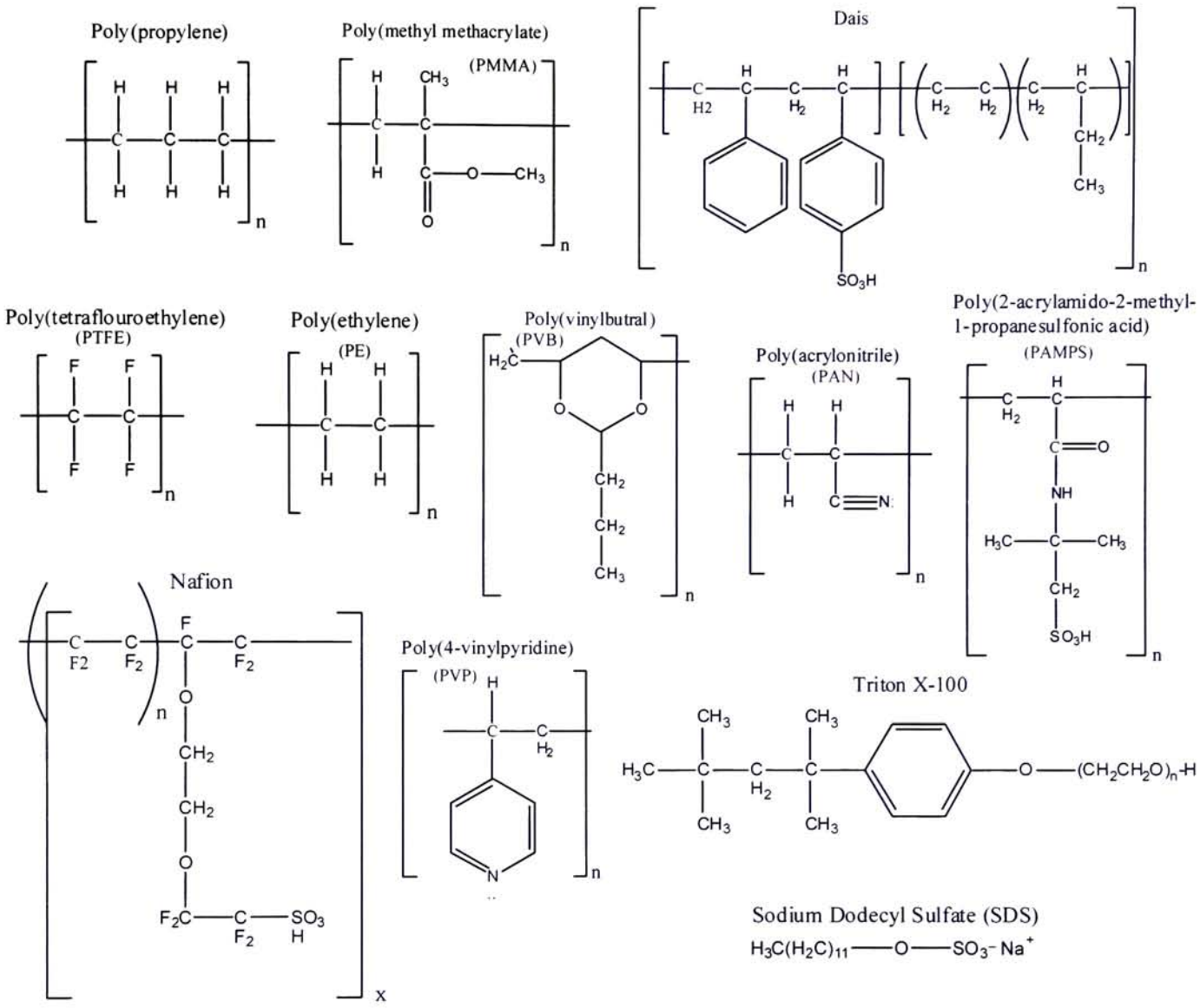

Figure 25: Structural Formulas of polymers and surfactants evaluated for homogeneous SWNT-polymer composite or SWNT-surfactant solutions. Polymers and surfactants designated in blue were successful dispersions.

blue are those, which have been observed as homogenous dispersions. Although there are variations in the degree of dispersion, homogeneity was evaluated by centrifugation, film casting, and optical absorption spectroscopy. The surfactant molecules shown: sodium dodecyl sulfate and Triton-X-100, displayed assisted dispersion of SWNTs into aqueous solutions, providing an aqueous system for potential fiber development. Each of the successful SWNT-polymer solutions from Figure 25, were evaluated with composite dispersions up to 5% w/w, with several up to 10% w/w, including Dais, Poly(acrylonitrile)-(PAN), and Poly(2-acrylamido-2-methyl-1-propanesulfonic acid)-(PAMPS). Nafion, the polymer selected for the complete actuator study in this project was successfully dispersed up to 18 % w/w. Comparison of conductivity between the successful composite dispersions may indicate which polymer systems can be potential composite actuators, dependent on the mechanism of actuation per polymer. Listed in **Table II** are four-point conductivity measurements for 3% w/w as-received h-SWNT-polymer composites. Interestingly, the Nafion composite exhibits the highest value from this composite study, followed by the PAMPS polymer.

Table II: Four-Point Probe Conductivity Measurements for 3% w/w h-SWNT-Polymer Composites

Polymer	Average Conductivity (S/cm)
Nafion	20.1
Poly(vinylbutyral)	0.00553
Poly(acrylonitrile)	0.0150
Poly(vinlypyridine)	1.93
Poly(2-acrylamido-2-methyl-1-propanesulfonic acid)	13.8

3.3 Characterization of Single Wall Carbon Nanotube-Polymer Composites

After dispersions of SWNT-polymer composites were reproducibly achieved, other studies were conducted to evaluate the effects SWNTs had on certain polymeric properties. Nafion was selected as the polymer of primary interest for evaluation of composite film conductivity and

optical spectroscopy effects. Since superior composite dispersions were achieved with Nafion and surface conductivities were also highest for this polymer system, it is imperative to thoroughly characterize this composite before actuator testing and analysis. The single wall carbon nanotube-Nafion composite series with varying percents by weight of purified h-SWNTs was evaluated for changes in conductivity following the procedure outlined in the *Experimental* section. Each of these composite films was analyzed using the four-point probe conductivity measurement and the results are presented in Figure 26. An overall exponential-like plot is observed with h-SWNT doping effects at ~5% w/w showing a significant enhancement of surface conductivity. Although this value appears to represent a percolation effect, corroboration of this threshold is beyond the scope of the project. It is certain that the h-SWNTs have a dramatic effect on the electrical conductivity over the surface of the Nafion composite films.

Investigation of the optical absorption spectra was performed to evaluate the effects of Nafion on SWNTs for 1% w/w h-SWNT and l-SWNT-Nafion composites. An overlay of the optical absorption spectra for purified h-SWNTs and the 1% w/w composite dispersion in Nafion is shown in Figure 27. The curves, normalized at 1025 nm, display a quenching of the absorption peak corresponding to the 1^{st} Van Hove singularity for the composite solution compared to the purified SWNTs. The specifics of these observed effects between h-SWNTs and the Nafion polymer is unclear and deferred to future studies. However, previous studies have shown quenching of this peak from pH effects,[69] alkali and halogen doping[62,63] and pressure effects.[70] Another possibility for absorption variation at the peak corresponding to the 1^{st} Van Hove singularity may be attributed to bundling effects, which have recently been predicted by theory.[71] Similar optical absorption results have also been observed for the 1% w/w l-SWNT-Nafion composites, Figure 28. The spectral overlay for purified l-SWNTs also shows quenching of the peak corresponding to the 1^{st} Van Hove singularity. The variations in signal intensity and peak

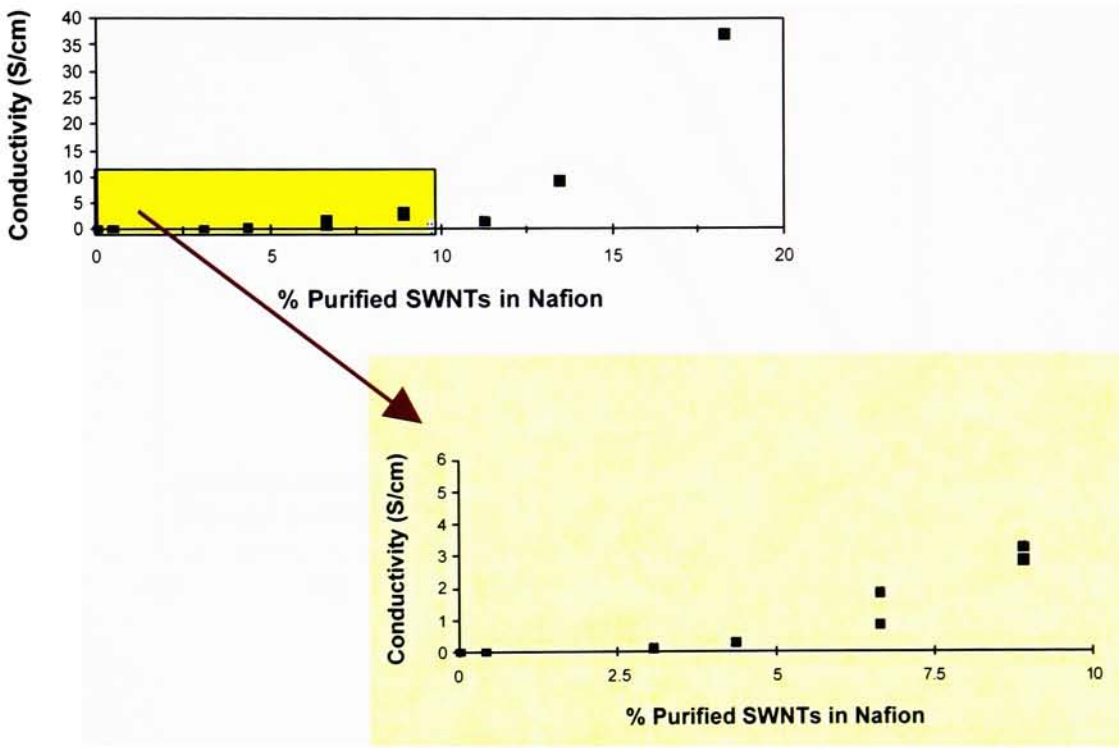

Figure 26: Plot of four-point probe conductivity measurements for the series of h-SWNT-Nafion composite films. Data indicates a percolation threshold of ~ 5% w/w from the inset graph for these films.

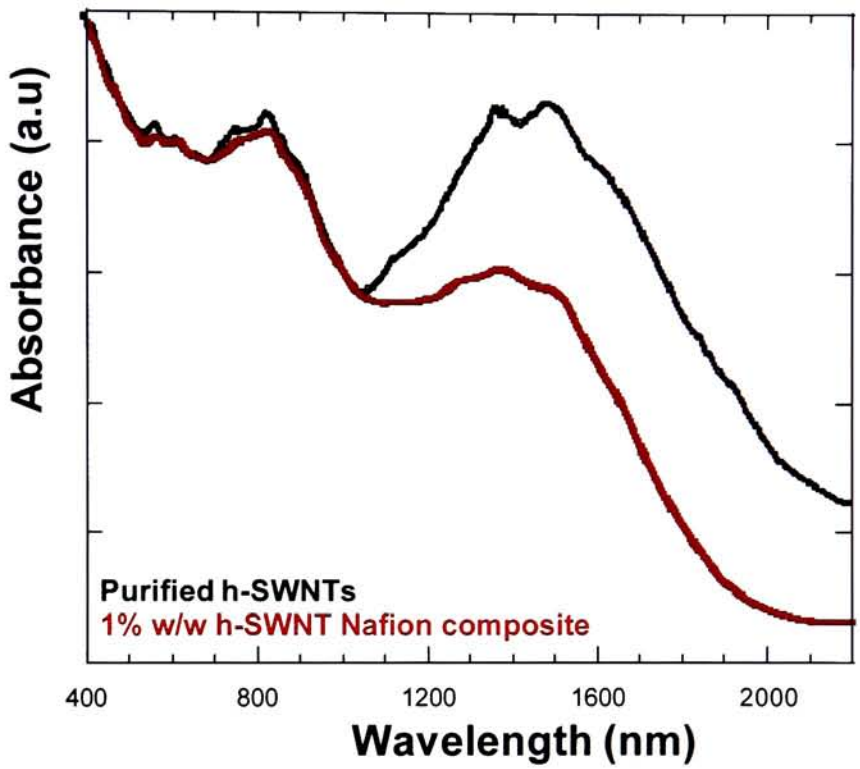

Figure 27: Optical Absorption overlay for purified, >95% w/w h-SWNTs, and 1% w/w purified h-SWNT-Nafion composite. Spectra normalized at 1025 nm. Relative peak ratios between 1st and 2nd Van Hove absorption peaks for purified h-SWNTs and 1% w/w purified h-SWNT-Nafion composite are 2.5, and 1.8, respectively.

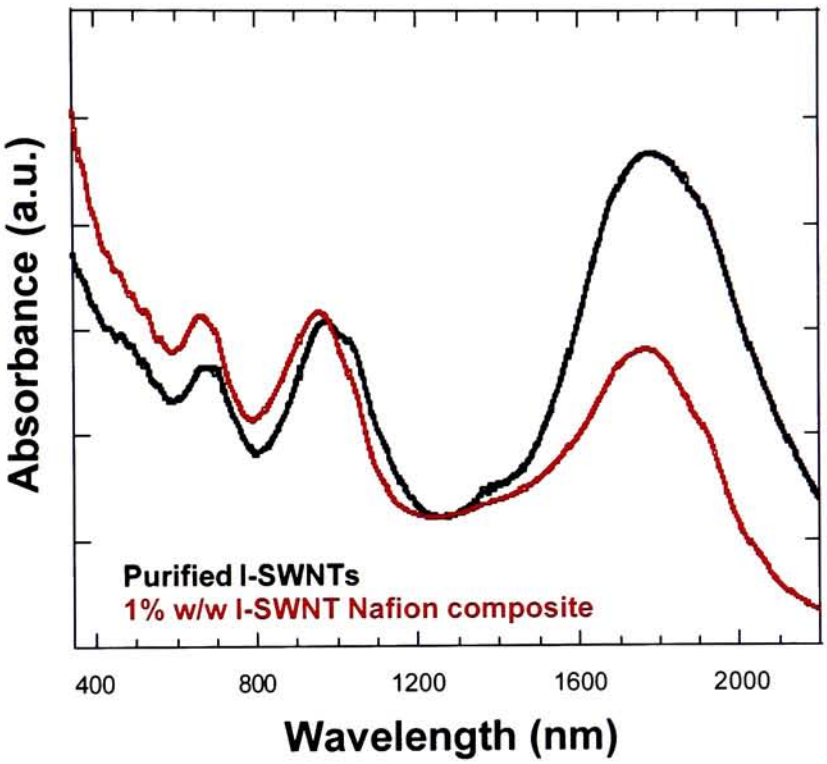

Figure 28: Optical Absorption overlay for purified, >95% w/w l-SWNTs, and 1% w/w purified l-SWNT-Nafion composite. Spectra normalized at 1250 nm. Relative peak ratios between 1st and 2nd Van Hove absorption peaks for purified l-SWNTs and 1% w/w purified l-SWNT-Nafion composite are 3.0, and 1.5, respectively.

resolution may be attributed to a preferential interaction of the Nafion with both h-SWNTs and l-SWNTs. In addition, bundling effects may be present, correlating to the theoretical predictions of peak broadening due to larger SWNT bundles.[71]

While optical absorption spectroscopy has displayed certain variations of the SWNT properties when dispersed in Nafion, these observations are insufficient to propose a definitive interaction between polymer and dopant. Microscopy analysis has however, shown an important conclusion which may lead to an accurate representation of the SWNT-Nafion interaction. While spectroscopy data may be supported by theoretical predictions, SEM images indicate a potential "debundling" of both the h-SWNTs and l-SWNTs when dispersed in Nafion. Figure 29 shows the comparison of purified h-SWNTs to a 10% w/w h-SWNT-Nafion composite film. The cross-sectional view of the composite shows the highly dispersed SWNT bundles protruding from the edge of the polymeric film. Microscopy analysis with statistical sampling of more than 20 bundles calculated the average bundle diameter in the purified h-SWNT paper to be 56 ± 13 nm (95% confidence). In comparison, the composite image represented average bundle diameters to equal 11 ± 1 nm (95% confidence). This five-fold decrease in bundle size correlates to an ~ 25-fold decrease in number of h-SWNTs per bundle.[72]

Although SWNT-Nafion composites were characterized more rigorously, other important data was acquired for SWNT-Dais composites. Optical absorption spectra were obtained for 1% w/w l-SWNT-Dais composites. Interesting effects of centrifugation are shown in Figure 30. The overlay plot shows the dramatic increase in resolution of the electronic transitions of the l-SWNTs evident from the fine structure of peaks, corresponding to each of the Van Hove singularities. Again, there is an observed reduction in broadness of the absorption at the 1st Van Hove peak to a more resolved one. Since the analysis is between high purity l-SWNTs and a centrifuged l-

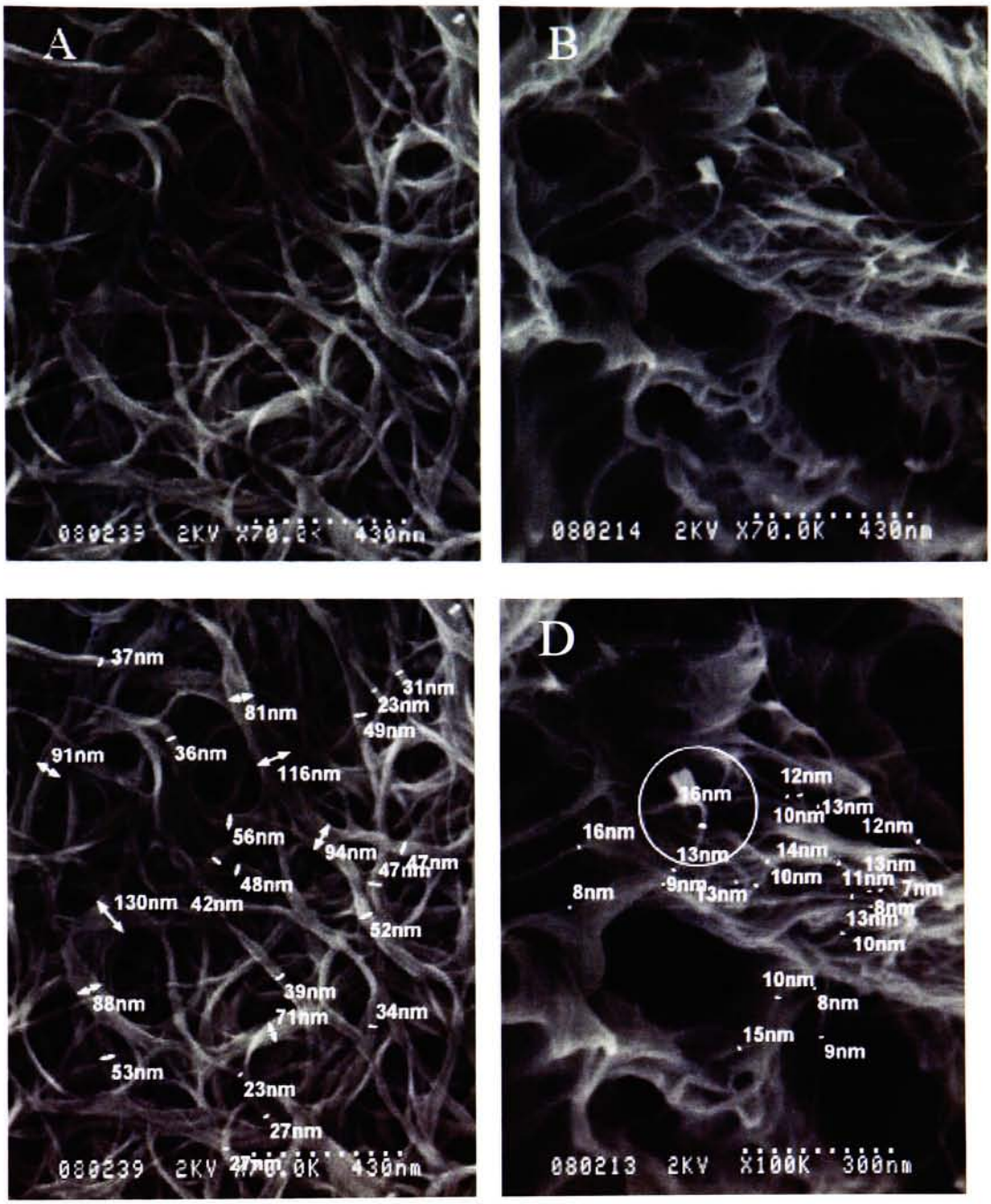

Figure 29: SEM image comparison of average bundle diameter of SWNTs upon dispersion of SWNTs into Nafion. The microscopy analysis displays (A) purified, >95% w/w h-SWNTs, (B) 10% w/w h-SWNT-Nafion composite, (C) diameter analysis of purified, and (D) diameter analysis of composite. Average SWNT bundle diameter from image (C) is 56 ± 13 nm and 11 ± 1 nm from image (D). Magnification at 70,000x for images A, B, and C; and 100,000x for image D.

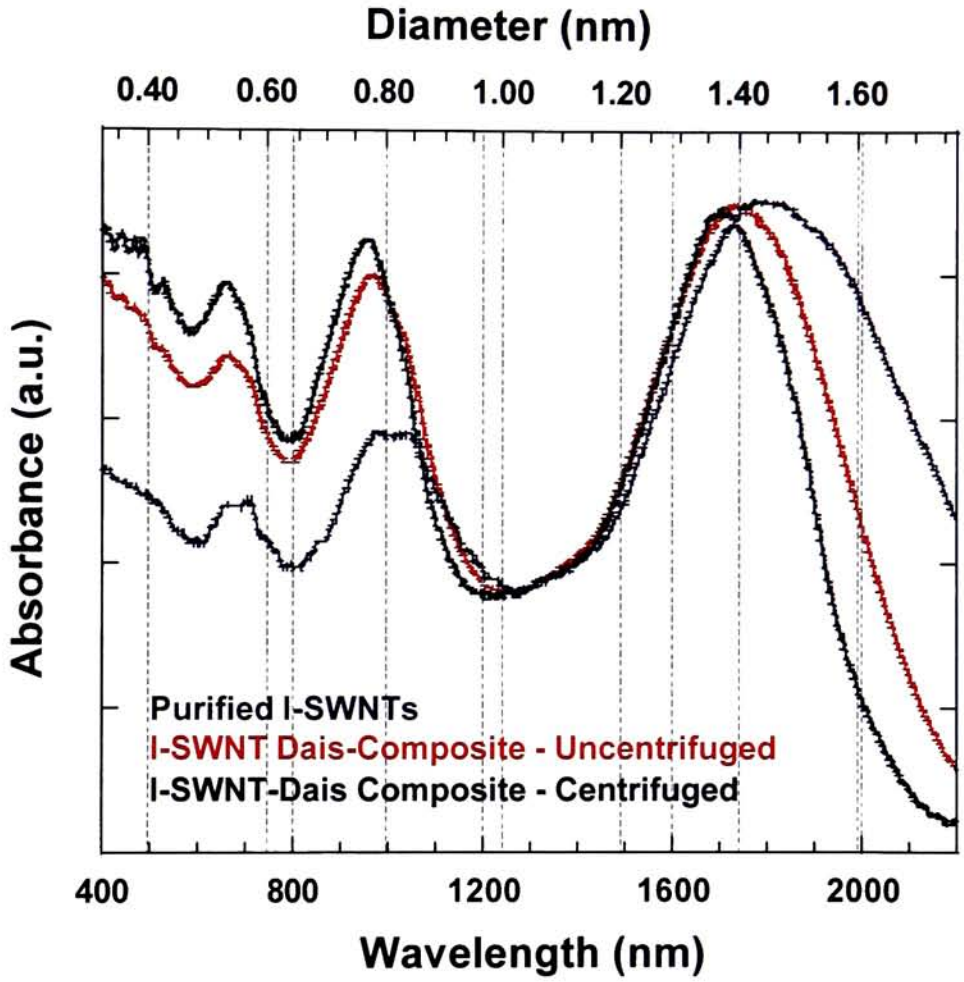

Figure 30: Optical Absorption overlay for purified, >95% w/w l-SWNTs, and 0.75% w/w purified l-SWNT-Dais composite (centrifuged and uncentrifuged). Spectra normalized at 1250 nm. Relative peak ratios between 1st and 2nd Van Hove absorption peaks for purified, uncentrifuged composite, and centrifuged composite are 2.7, 2.0, and 1.9, respectively.

SWNT-Dais composite, the results may correspond to the debundling effects predicted by theory and preliminarily proposed with the SWNT-Nafion composites.

3.4 Evaluation of Single Wall Carbon Nanotube-Polymer Composite Actuators

Single wall carbon nanotube-polymer composites were each tested for actuator response using the bimorph cantilever actuator setup described by Baughman et. al.[5] Evaluation of each of the successful dispersions of SWNT-polymer solutions shown in Figure 25, concluded that Nafion was the only viable polymer for actuation at low SWNT doping levels, <10% w/w. Since Nafion has been reported by many groups to actuate when doped with high percent by weights of noble metals, it was necessary to evaluate whether the SWNTs were acting as a conductive network to promote Nafion actuation, SWNTs were actuating independently, or both SWNTs and Nafion were actuating concertedly.

As seen in Figure 26, the conductivity of the series of h-SWNT-Nafion polymer composite films increases exponentially. To eliminate surface conductivity effects due to the resistive losses over the surface of the film during actuator testing, a limited platinization process was employed to establish a uniform contact between samples. This platinization process reproducibly resulted in a platinum coating on the Nafion membrane to be ~ 0.1 microns as determined by SEM (Figure 31). The resistivity of the films was a consistent 0.1 ohm*cm for platinized Nafion composites. Even though the nanotube doped membranes with > 5% w/w SWNTs resulted in films with similar conductivity without platinization, they were platinized in order to maintain consistency in the experimental measurements. The corresponding plot for conductivity of the h-SWNT-Nafion composite series after the platinization procedure is shown in Figure 32. The percents by weight of h-SWNTs have been adjusted for the added platinum mass.

Analysis of each percent by weight SWNT doped Nafion composite actuator was performed using the optical displacement analysis described in the *Experimental.* It was shown that both

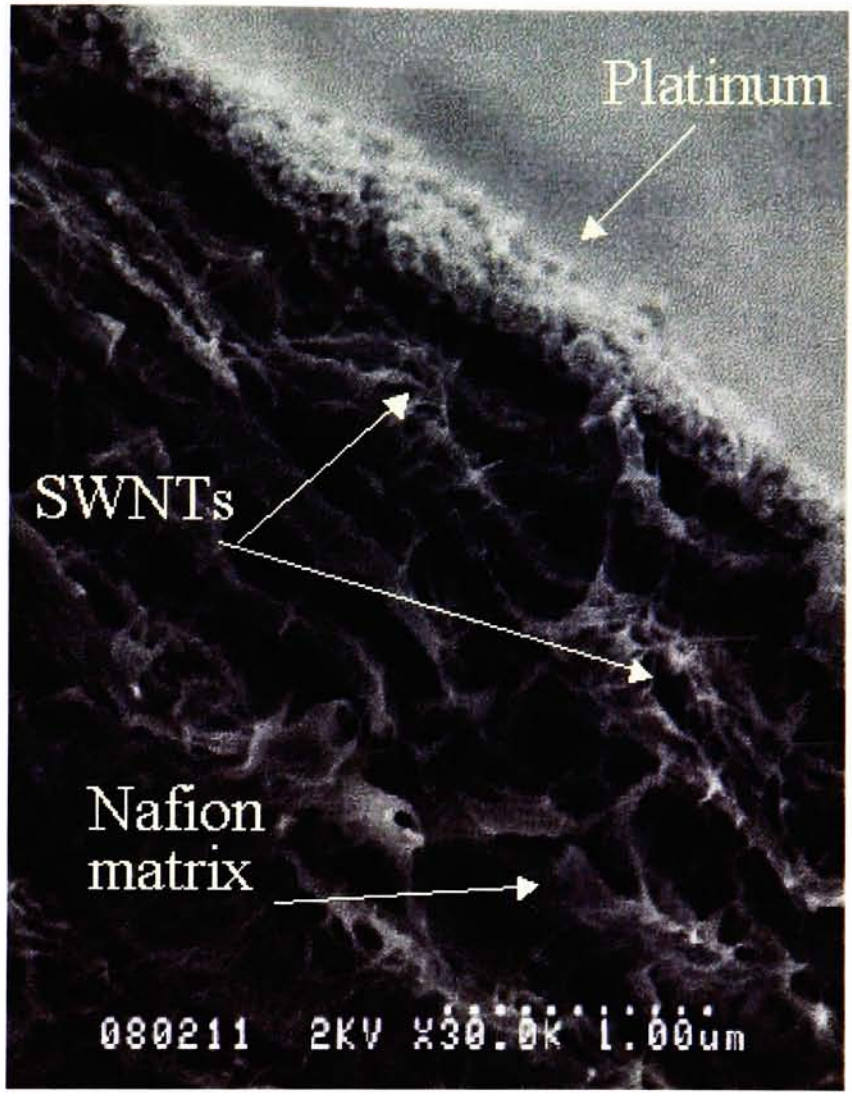

Figure 31: SEM image providing cross-sectional view of a platinized h-SWNT-Nafion composite film. Designation of the platinum, h-SWNTs, and nafion matrix is shown. Magnification at 30,000x.

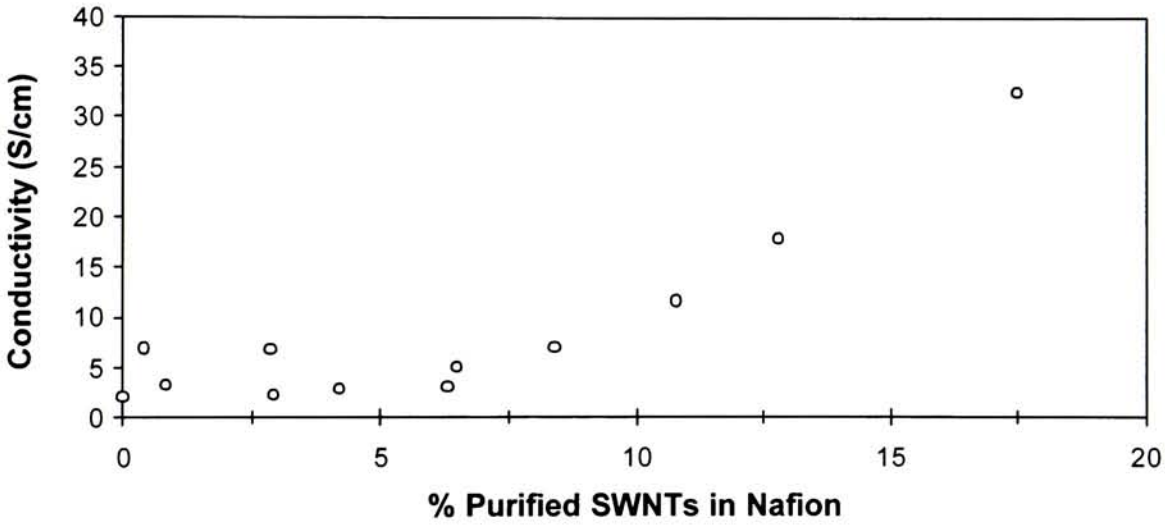

Figure 32: Plot of four-point probe conductivity measurements for the series of platinized h-SWNT-Nafion composite films. Data is constant until ~5% w/w, when significant increase in conductivity is observed.

excitation step voltages and frequencies altered the cantilever tip response. When the frequency was doubled, typical trials displayed between 50-60% of maximum displacement. The complete data set for all analyzed actuators by this method is included in Figure 33. Bimorph cantilever actuators prepared with as-received h-SWNTs (buckeypaper constructed from filtration of SWNTs suspended in 1 M HCl solution) displayed displacement responses less than any of the measured purified h-SWNT-Nafion composite actuators, including the 0.41% w/w sample. While this result requires further study, the notion of as-produced h-SWNT actuators being inferior to h-SWNT-Nafion composite actuators in aqueous electrolyte solutions is plausible since the mechanism supporting Nafion actuation cites the important effects of water on enhancing the generated response. Since fresh, newly prepared, h-SWNT-Nafion composite actuators showed remarkable results, the practicality of storage and repeated use was also investigated. When composite actuators were stored at room temperature in open air without any treatment (i.e. rinsing of $LiCl_{(aq)}$ solution from sample), the actuator response was significantly reduced. Evaluation of the 8.4 % w/w h-SWNT-Nafion composite actuator when stored in distilled water for 1 week showed a decrease in actuator response by 60%. However, if maintained in the $LiCl_{(aq)}$ solution for comparable storage times, the actuator response was not affected.

Comparison of the actuator response for SWNTs dispersed in Nafion resulting from two different synthetic routes (i.e. pulse laser vaporization and HiPco), was also investigated. Displacement measurements were observed for 3% w/w l-SWNT and h-SWNT-Nafion composite actuators to equal ~0.3 mm at ± 2.0 V excitation and a frequency of 1 Hz. Interestingly, this preliminary result shows no significant change in actuation based on variation in diameter distribution for SWNTs dispersed in Nafion, although future work is necessary to support this observation.

Voltage (±) V	Frequency (Hz)	Displacement (mm)
	0.41 % w/w h-SWNTs	
2.0 V	1.0	0.190
2.0 V	2.0	0.060
	0.84 % w/w h-SWNTs	
2.0 V	1.0	0.730
2.0 V	2.0	0.330
	2.86 % w/w h-SWNTs	
0.5 V	1.0	0.100
1.0 V	1.0	0.480
1.0 V	2.0	0.330
2.0 V	1.0	1.210
2.0 V	2.0	0.650
2.0 V	5.0	0.140
	2.93 % w/w h-SWNTs	
0.5 V	1.0	0.050
1.0 V	1.0	0.100
1.0 V	2.0	0.080
2.0 V	1.0	0.300
2.0 V	2.0	0.240
	4.21 % w/w h-SWNTs	
0.5 V	1.0	0.160
1.0 V	1.0	0.320
1.0 V	2.0	0.290
2.0 V	1.0	2.090
2.0 V	2.0	1.110
	6.32 % w/w h-SWNTs	
0.25 V	1.0	0.080
0.5 V	1.0	0.140
1.0 V	1.0	0.330
1.0 V	2.0	0.140
2.0 V	1.0	0.560
2.0 V	2.0	0.380
2.0 V	5.0	0.080
	6.49 % w/w h-SWNTs	
0.5 V	1.0	0.200
1.0 V	1.0	0.520
1.0 V	2.0	0.240
2.0 V	1.0	1.690
2.0 V	2.0	1.120
	8.41 % w/w h-SWNTs	
0.2 V	1.0	0.060
0.5 V	1.0	0.200
1.0 V	1.0	0.360
1.0 V	2.0	0.190
2.0 V	1.0	0.680
2.0 V	2.0	0.340
2.0 V	5.0	0.170

Voltage (±) V	Frequency (Hz)	Displacement (mm)
	8.41 % w/w h-SWNTs sample stored for 1 week in H2O	
2.0 V	1.0	0.280
2.0 V	2.0	0.160
1.0 V	1.0	0.150
1.0 V	2.0	0.080
	10.8 % w/w h-SWNTs	
0.025 V	1.0	0.030
0.05 V	1.0	0.040
0.1 V	1.0	0.090
0.25 V	1.0	0.170
0.5 V	1.0	0.330
1.0 V	1.0	0.610
1.0 V	2.0	0.410
2.0 V	1.0	1.070
2.0 V	2.0	0.510
2.0 V	5.0	0.250
	12.8 % w/w h-SWNTs	
0.5 V	1.0	0.250
0.5 V	2.0	0.160
1.0 V	1.0	0.430
1.0 V	2.0	0.240
2.0 V	1.0	1.190
2.0 V	2.0	0.710
2.0 V	5.0	0.700
	17.5 % w/w h-SWNTs	
0.5 V	1.0	0.620
0.5 V	2.0	0.410
1.0 V	1.0	1.850
1.0 V	2.0	1.120
2.0 V	1.0	4.450
2.0 V	2.0	2.710
2.0 V	5.0	1.450
	As-received h-SWNTs	
0.5 V	1.0	0.110
1.0 V	1.0	0.200
2.0 V	1.0	0.230
2.0 V	2.0	0.160
2.0 V	5.0	0.060
	3.10 % w/w l-SWNTs	
1.0 V	1.0	0.160
1.0 V	2.0	0.090
2.0 V	1.0	0.310
2.0 V	2.0	0.210

Figure 33: Overview of data for h-SWNT-Nafion composite actuator study. The experimental excitation conditions (applied voltages and operating frequencies) are listed for each composite along with corresponding displacement values.

The series of results for the varying percents by weight SWNT-Nafion composite actuators was evaluated at the different experimental conditions. Figure 34 shows the graphical representation of the displacement (mm) versus the SWNT doping level in Nafion for the largest observed actuation: an excitation step voltage of ± 2.0 V and frequency of 1 Hz. While there is a general trend of the displacement response to increase with higher doping levels, there is scatter between the data points. Normalization of this data with the composite film's conductivity from Figure 32, produces a relatively constant response (Figure 35). This leads one to propose a direct relationship between displacement and film conductivity for SWNT-Nafion composite actuators. Results at different excitation conditions show similar displacement effects, although the displacement values are substantially less. Figure 36 shows the displacement data at ± 0.5 V and frequency of 1 Hz. Similarly, Figure 37 depicts the displacement data at ± 1.0 V and frequency of 1 Hz, with the significant effect being higher values compared to ± 0.5 V. If the frequency is doubled, as shown in Figure 38 for ± 1.0 V, there is a reduction in displacement by approximately 50%. A similar comparison was made at ± 2.0 V for frequency, namely Figure 34 at 1 Hz, compared to Figures 39 and 40, at 2 and 5 Hz, respectively. Again, there is an approximate reduction by 50% as the frequency doubles. Overall, the general trend in each plot however, is an increase in cantilever tip deflection as the SWNT doping level is corresponding increased.

The effect of excitation voltage on displacement is shown for the 10.8% w/w SWNT-Nafion composite actuator in Figure 41. There is a linear-like relationship for the excitation voltage on cantilever tip displacement, although additional data points would be necessary to confirm this relationship. However, it seems plausible from this data that the general scatter observed in the deflection plots is a result of differences between actuator samples. These deviations could be attributed to variations in surface conductivity between composite films, different adhesion to the polyimide substrate, or disparities in the differential expansion during ion intercalation. Further

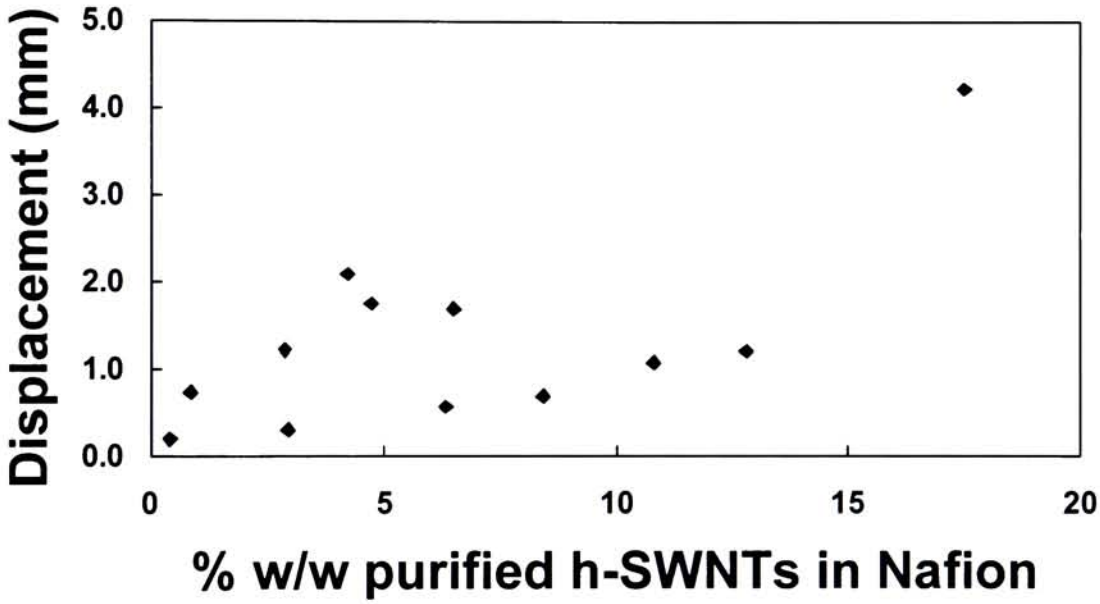

Figure 34: Deflection data for h-SWNT-Nafion composite actuators. Measured displacement of actuator cantilever tip at ±2.0 V applied excitation and 1 Hz operating frequency.

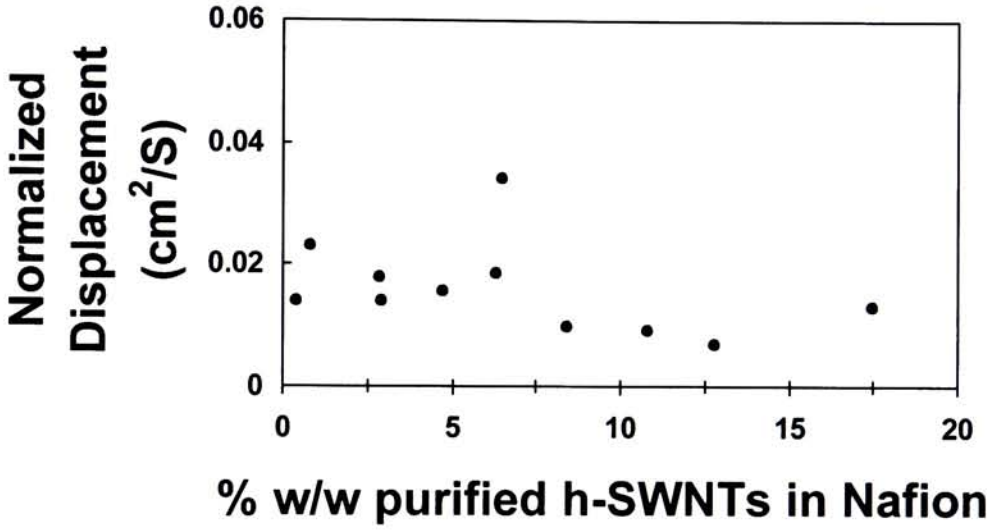

Figure 35: Normalized deflection data for h-SWNT-Nafion composite actuators from Figure 33 with four-point conductivity values from Figure 31.

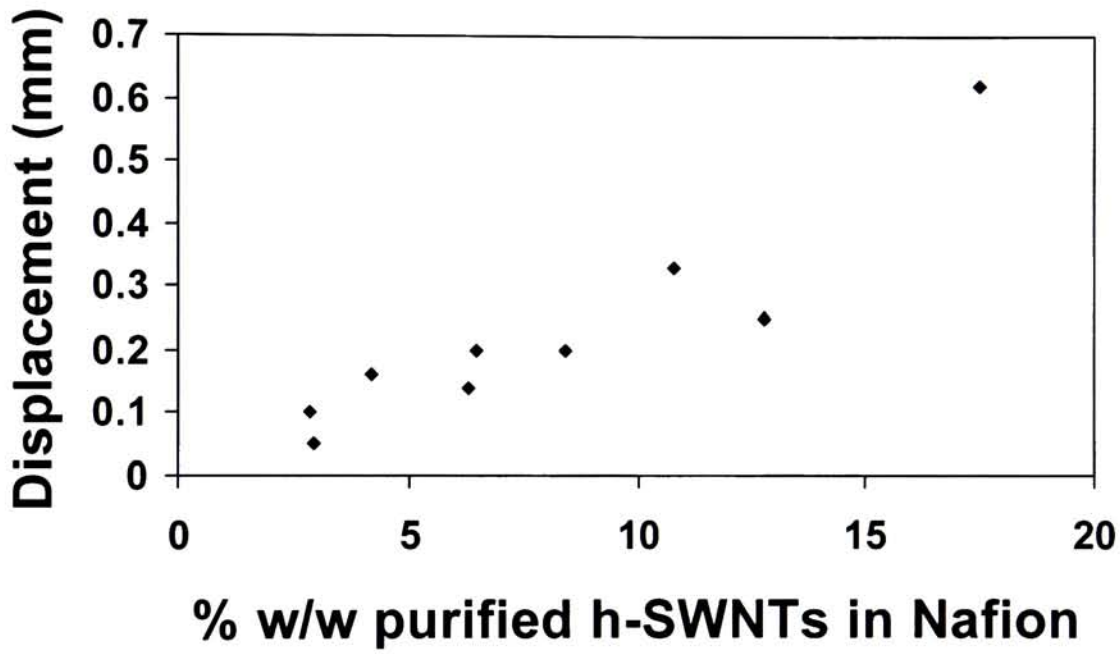

Figure 36: Deflection data for h-SWNT-Nafion composite actuators. Measured displacement of actuator cantilever tip at ±0.5 V applied excitation and 1 Hz operating frequency.

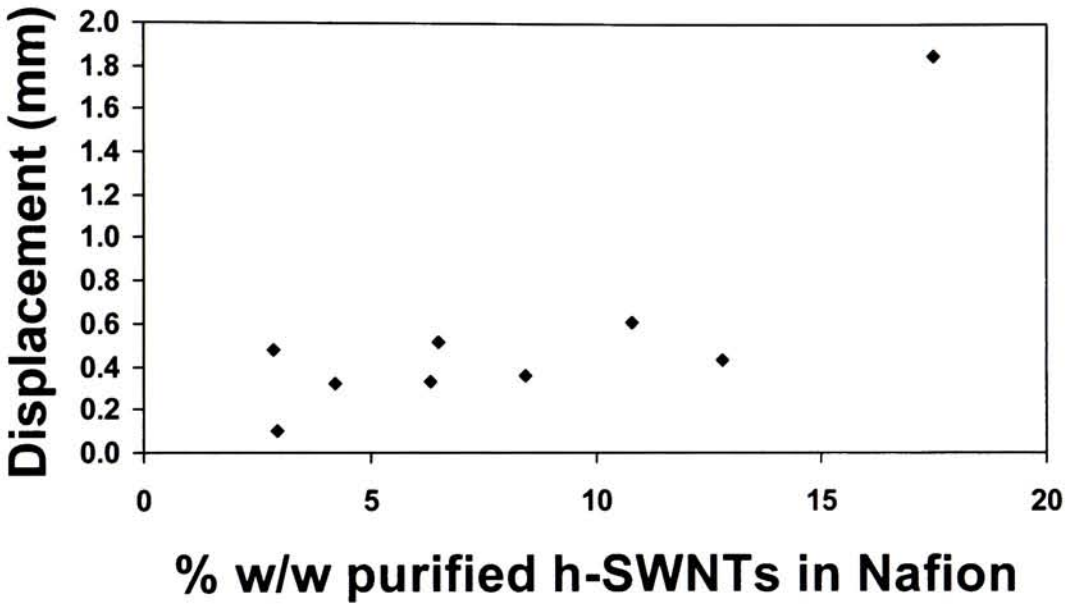

Figure 37: Deflection data for h-SWNT-Nafion composite actuators. Measured displacement of actuator cantilever tip at ±1.0 V applied excitation and 1 Hz operating frequency.

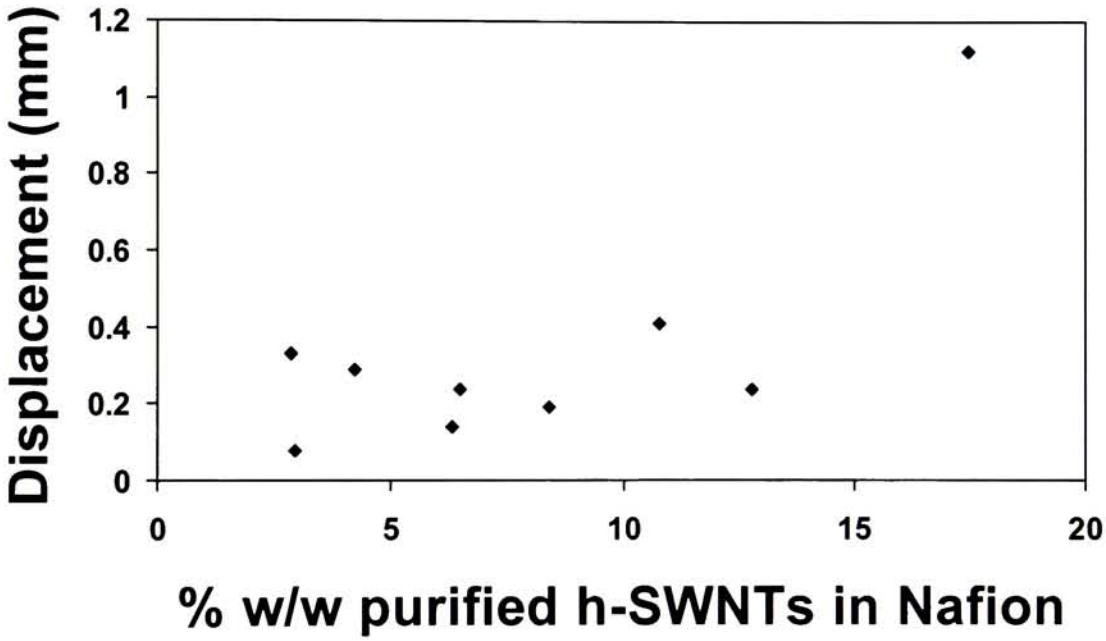

Figure 38: Deflection data for h-SWNT-Nafion composite actuators. Measured displacement of actuator cantilever tip at ±1.0 V applied excitation and 2 Hz operating frequency.

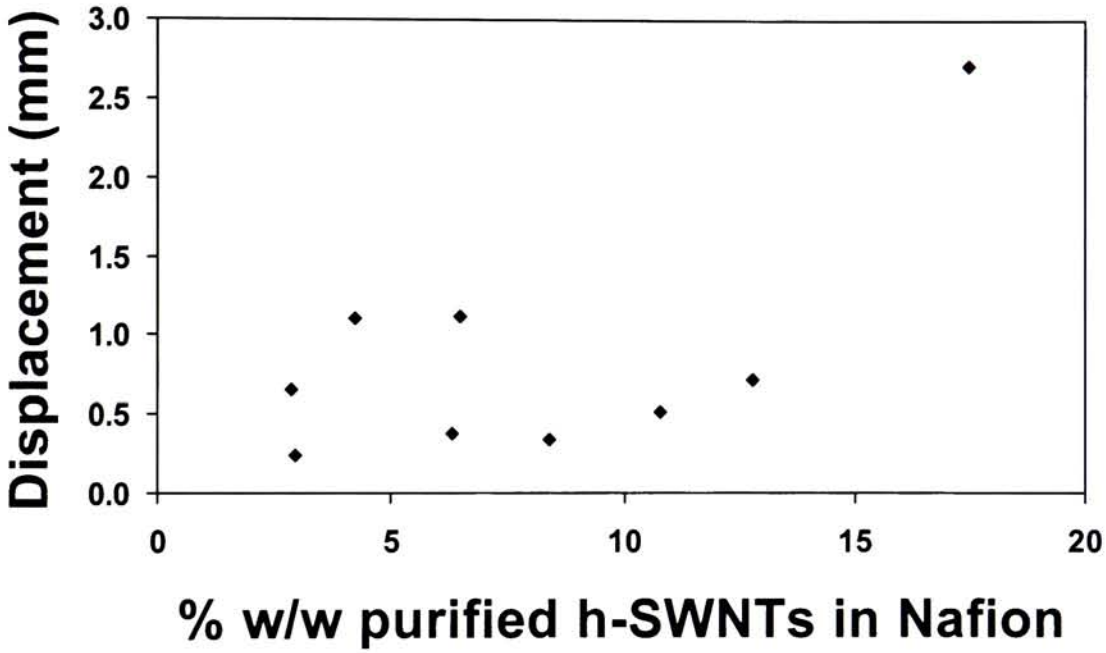

Figure 39: Deflection data for h-SWNT-Nafion composite actuators. Measured displacement of actuator cantilever tip at ±2.0 V applied excitation and 2 Hz operating frequency.

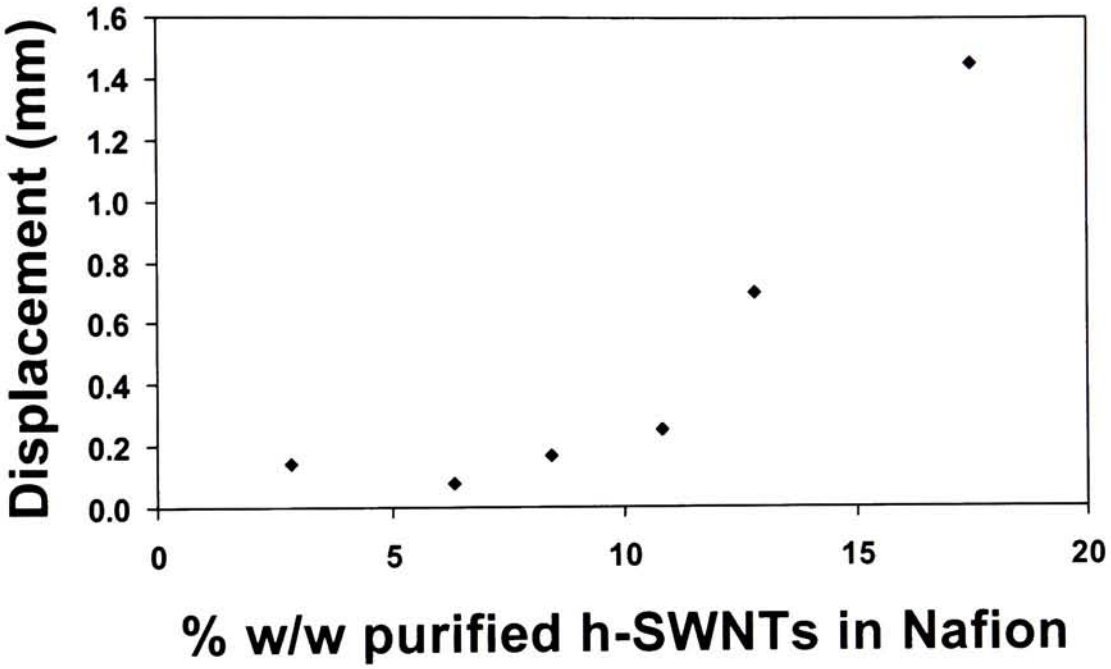

Figure 40: Deflection data for h-SWNT-Nafion composite actuators. Measured displacement of actuator cantilever tip at ±2.0 V applied excitation and 5 Hz operating frequency.

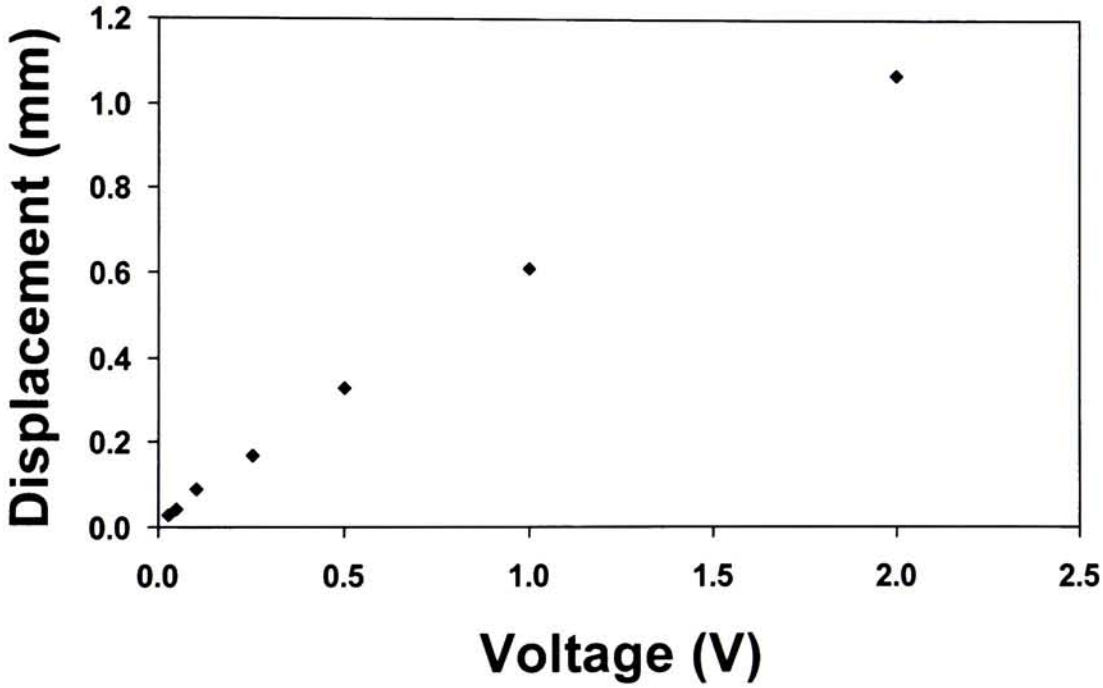

Figure 41: Deflection data for the 10.8 % w/w h-SWNT-Nafion composite actuators as a function of excitation voltage. Shown is the relationship of applied excitation voltages on the actuator cantilever tip displacement at 1 Hz operating frequency.

analysis of excitation voltages and frequency effects on SWNT dopings could lead to optimization of the actuator response for SWNT-Nafion composite actuators.

Another important observation for each of the h-SWNT-Nafion composite actuators > 1% w/w, was the lack of relaxation of the cantilever tip, post-excitation. Abe et. al., has reported relaxation of the cantilever tip due to osmotic effects back to initial state in <10 seconds.[6] The SWNT-Nafion composite actuators did not exhibit such properties. Single wall carbon nanotubes may alter the water content properties in Nafion films by reducing ionic mobility or dehydrating the ionic clusters, due to the hydrophobicity of SWNTs.

Results indicate that the mechanism for SWNT-Nafion composite actuation is similar to that reported for metal-doped Nafion actuators. Under a potential bias, solvated cations intercalate into the Nafion matrix. This ion intercalation is enhanced for the SWNT-Nafion composite films by the dispersed SWNTs, which form a highly conductive percolation network. The solvated cations induce cathode expansion, which leads to differential expansion of the electrodes, and bending towards the anode. Reversal of the potential will result in ion intercalation at the opposite electrode, causing an overall device actuation if the potential bias is continuously alternated between electrodes. The unique benefit of dispersed SWNTs within the Nafion matrix is conductivity throughout the entire film. Application of these results to future research may allow for development of highly efficient, SWNT-Nafion composite actuators.

4.0 Conclusion

Successful incorporation of single wall carbon nanotubes into a polymer matrix resulted in novel actuators, requiring significant steps involved with purification, characterization, and analysis of the SWNT dopant material. Additionally, techniques required to efficiently disperse the SWNTs into polymer matrices were also developed. Protocols were established to consistently purify as-produced SWNTs either from commercial sources like Carbon Nanotechnologies Inc., or in-house laser procedures, at purities >95% w/w. Upon characterization of these SWNT materials, dispersion into various polymer matrices was consistently achieved. Specifically, SWNT-Nafion composites were produced at doping levels up to 18% w/w. Interestingly, a significant "debundling" effect was observed with SWNT-Nafion composites, displaying reduction of average bundle diameters by a factor of five for the h-SWNT-Nafion composite films.

Single wall carbon nanotube-Nafion composite actuators were demonstrated with maximum observed displacements for the platinized 17.5% w/w SWNT-Nafion composite film equal to 4.5 mm at ± 2.0 V and 1 Hz. Moreover, no relaxation of the cantilever tip was observed for the SWNT-Nafion composite actuators. Normalization of the actuator tip displacement to composite conductivity showed the direct relationship of conductivity on deflection for SWNT-Nafion composite actuators. The percolation of the electrically conductive, high aspect ratio SWNTs, enables a dramatic increase in the conductivity of the composite films. This property manifests into superior actuation at low doping levels of SWNTs in Nafion, observing equivalent actuation responses to the > 30% w/w noble metal-doped Nafion actuators. The use of SWNTs can promote a higher degree of intercalation, rather than limited intercalation when only the surface of the electrode film is conductive, as with the noble metal-Nafion actuators. Therefore, by using SWNTs, greater actuator deflections are potentially possible since higher degrees of solvated cation intercalation would lead to an increase in differential expansion between electrodes. Based

on this initial study,[73] a couple of considerations have to be made to confirm this proposition, namely, controlling the metallic:semiconductor ratio of the SWNTs, and production of higher doped SWNT-Nafion composite actuators. The relative ratios of SWNT types were not investigated, but have been reported to be ~2/3 semiconducting SWNTs in the as-produced material.[66] Variations on synthesis leading to phase-pure metallic SWNTs would be advantageous to higher composite conductivities, lowering SWNT percolation thresholds, and potentially producing better SWNT-Nafion composite actuators. Overall, the incorporation of SWNTs into a polymer matrix has been demonstrated and characterized for a novel device, namely an efficient SWNT-Nafion composite actuator.

5.0 Appendix

5.1 Preparation of SWNT-Polymer Composite Fibers

In addition to characterization of other SWNT-polymer composites, attempts to develop SWNT-polymer fibers were also investigated. Single wall carbon nanotube-polymer composite solutions were extruded from dispersed solutions into an extruding solvent, typically propylene glycol. Fiber extrusion using the SWNT-Polymer composite solutions was achieved using a 50 μL syringe. Elution of the composite solution into selected extruding solvents, dependent on the composite polymer solvent, occurred to prevent solubility. Various percent by weight composite solutions were prepared in either polymeric or surfactant systems using Equation **1**. Extruding rates varied depending on the type and stability of SWNT-Polymer composite fibers, while extrusion was manually controlled. Exploitation of polarity effects between solvents was the driving force for fiber formation. While several attempts were fruitful, others were unable to be removed from the extruding solvent. Evaluation of the complete study is shown in **Table III**, indicating the SWNT content, polymer type, and fiber result.

Data from **Table III** indicates that composites of PAN and PVB were most successful for producing SWNT-polymeric fibers. The dispersions of PMMA were not homogeneous and the resultant fiber was formed from coagulation of the as-produced h-SWNTs, which were previously reported to contain substantial amounts of carbonaceous impurities. Although fibers were achieved, removal of the propylene glycol coating would be essential before actuator experiments could be performed. While this data reflects preliminary success in fiber development, future work designed to produce conductive SWNT-polymeric fibers and ribbons may lead to advances in microactuators.

Table III: Fiber Extrusion Attempts with SWNT-Polymer Composite Dispersions

SWNT Type[1]	Polymer/Solvent	Extruding Solvent	Result[2]
10% w/w a-h-SWNTs	Nafion/Ethanol	Propylene Glycol	No Fiber
10% w/w a-h-SWNTs	PMMA/DMF[3]	Propylene Glycol	Fiber formed but coated
1% w/w p-l-SWNTs	PMMA/DMF[3]	Propylene Glycol	No dispersion-formed a monolayer film
4% w/w a-l-SWNTs	PVB/Isopropanol	Propylene Glycol	Thick-irregular fibers
4% w/w p-l-SWNTs	PAN/DMF	Propylene Glycol	Thin-short fibers
10% w/w a-h-SWNTs	PAN/DMF	Propylene Glycol	Thin-short fibers
10% w/w a-h-SWNTs	PAMPS/Water	Hexanes	Fiber formed in solution – unable to be removed
10% w/w a-h-SWNTs	PAMPS/Water	Propylene Glycol	Composite solution adsorbed to glass surface
0.1% w/w p-h-SWNTs	2% SDS/Water	Propylene Glycol	No Fiber
0.1% w/w p-h-SWNTs	2% Triton –X/Water	Propylene Glycol	No Fiber
0.1% w/w p-h-SWNTs	2% Triton –X/Water	5% PVA in Water[4]	Fiber with PVA coating-unable to be removed
5% w/w a-h-SWNTs	Dais/2-Propanol	Propylene Glycol	No fiber

[1]The SWNT type is either designated (a-) for as-produced or (p-) for purified

[2]Results in red were successful fibers

[3]Dimethylformamide – (DMF)

[4]5% w/w Poly(vinyl alcohol) – (PVA) in water

6.0 References

(1) Che, G., Miller, S.A., Fisher, E.R., Martin, C.R. *Anal. Chem.* **1999**, *71*, 3187-3191.

(2) Baughman, R. *Synth. Met.* **1996**, *78*, 339-353.

(3) Bay, L., Jacobsen, T., Skaarup, S., West, K. *J. Phys. Chem. B* **2001**, *105*, 8492-8497.

(4) Sonoda, Y., Takashima, W., Kaneto, K. *Synth. Met.* **2001**, *119*, 267-268.

(5) Baughman, R.; Cui, C.; Zakhidov, A. A.; Iqbal, Z. B., J.N.; Spinks, G.M.; Wallace, G.G.; Mazzoldi, A.; De Rossi, D.; Rinzler, A.G.; Jaschinski, O.; Roth, S.; Kertesz, M. *Science* **1999**, *284*, 1340-1344.

(6) Abe, Y., Mochizuki, A.; Kawashima, T.; Yamashita, S.; Asaka, K.; Oguro, K. *Polym. Adv. Technol.* **1998**, *9*, 520-526.

(7) Shahinpoor, M. In *Proc. SPIE: Smart Materials*; Wilson, A. R. A., H., Ed., 2001; Vol. 4234, pp 203-214.

(8) Schreyer, H. B., Gebhart, N., Kim, K.J., Shahinpoor, M. *Biomacromolecules* **2000**, *1*, 642-647.

(9) Irvin, D. J., Goods, S.H., Whinnery, L.L. *Chem. Mater.* **2001**, *13*, 1143-1145.

(10) Eisenberg, A., Yeager, H.L. *Perfluorinated Ionomer Membranes*; American Chemical Society: Washington, D.C., 1982.

(11) Kim, K. J., Shahinpoor, M. *Polymer* **2002**, *43*, 797-802.

(12) Noh, T. G., Tak, Y., Nam, J.D., Choi, H. *Electrochimica Acta* **2002**, *00*, 1-6.

(13) Fujiwara, N., Asaka, K., Nishimura, Y., Oguro, K., Torikai, E. *Chem. Mater.* **2000**, *12*, 1750-1754.

(14) Onishi, K., Sewa, S., Asaka, K., Fujiwara, N., Oguro, K. *Electrochimica Acta* **2001**, *46*, 1233-1241.

(15) Uchida, M., Taya, M. *Polymer* **2001**, *42*, 9281-9285.

(16) Asaka, K., Fujiwara, N., Oguro, K., Onishi, K., Sewa, S. *J. Electroanal. Chem.* **2001**, *505*, 24-32.

(17) Spinks, G. M., Wallace, G.G., Fifield, L.S., Dalton, L.R., Mazzoldi, A., De Rossi, D., Khayrullin, I.I., Baughman, R.H. In *Mat. Res. Soc. Symp. Proc.*, 2002; Vol. 706.

(18) Fraysse, J., Minett, A.I., Gu, G., Roth, S., Rinzler, A.G., Baughman, R.H. *Curr. Appl. Phys.* **2001**, *1*, 407-411.

(19) Minett, A., Fraysse, J., Gang, G., Kim, G.T., Roth, S. *Curr. Appl. Phys.* **2002**, *2*, 61-64.

(20) Ajayan, P. M. *Chem. Rev.* **1999**, *99*, 1787-1799.

(21) Forro, L., Schonenberger, C. In *Carbon Nanotubes Synthesis, Structure, Properties, and Applications*; Dresselhaus, M. S. D., G.; Avouris, Ph., Ed.; Springer: New York, 2000; Vol. 80, pp 329-390.

(22) Jacques, D., Villain, S.; Rao, A.M.; Andrews, R.; Derbyshire, F.; Dickey, E.C.; Qian, D. In *Amorphous and Nanostructured Carbon*; Sullivan, J. P., et. al., Ed.; Materials Research Society: Warrendale, 2000; Vol. 593, pp 15-20.

(23) Jin, L., Bower, C.; Zhou, O. *Appl. Phys. Lett.* **1998**, *73*, 1197-1199.

(24) Srivastava, D., Brenner, D.W.; Schall, J.D.; Ausman, K.D.; Yu, M.; Ruoff, R.S. *J. Phys. Chem. B* **1999**, *103*, 4330-4337.

(25) Frank, S. *Science* **1998**, *280*, 1744-1746.

(26) Schonenberger, C., Forro, L. In *Physics World*, 2000, pp 37-42.

(27) Cumings, J. *Nature* **2000**, *406*, 586.

(28) Dai, L., Mau, A.W.H. *Adv. Mater.* **2001**, *13*, 899-913.

(29) Odom, T. W., Huang, J.; Kim, P.; Lieber, C.M. *J. Phys. Chem. B* **2000**, *104*, 2794-2809.

(30) Nikolaev, P., Bronikowski, M.J., Bradley, R.K., Rohmund, F., Colbert, D.T., Smith, K.A., Smalley, R.E. *Chem. Phys. Lett.* **1999**, *313*, 91-97.

(31) Rinzler, A. G., Liu, J.; Dai, H.; Nikolaev, P.; Huffman, C.B.; Rodriguez-Macias, F.J.; Boul, P.J.; Lu, A.H.; Heymann, D.; Colbert, D.T.; Lee, R.S.; Fischer, J.E.; Rao, A.M.; Eklund, P.C.; Smalley, R.E. *Appl. Phys. A* **1998**, *67*, 29-37.

(32) Wang, N., Tang, Z.K.; Li, G.D.; Chen, J.S. *Nature* **2000**, *408*, 50-51.

(33) Peng, H. Y., Wang, N.; Zheng. Y.F.; Lifshitz, Y.; Kulik, J.; Zhang, R.Q.; Lee, C.S.; Lee, S.T. *Appl. Phys. Lett.* **2000**, *77*, 2831-2833.
(34) Qin, L., Zhao, Z.; Hirahara, K.; Miyamoto, Y.A.; Iijima, S. *Nature* **2000**, *408*, 50.
(35) McEuen, P. L. In *Physics World*, 2000, pp 31-36.
(36) Collins, P. G., Avouris, P. In *Scientific American*, 2000; Vol. 283, pp 62-69.
(37) Esfarjani, K., Farajian, A.A.; Hashi, Y.; Kawazoe, Y. *Appl. Phys. Lett.* **1999**, *74*, 79-81.
(38) Gennett, T., Dillon, A.C.; Alleman, J.L.; Jones, K.M.; Hasoon, F.S.; Heben, M.J. *Chem. Mater.* **2000**, *12*, 599-601.
(39) Thostenson, E. T., Ren, Z.; Chou, T. *Composites Science and Technology* **2001**, *61*, 1899-1912.
(40) Yao, N., Lordi, V. *J. Appl. Phys.* **1998**, *84*, 1939-1943.
(41) Li, F., Cheng, H.M.; Bai, S.; Su, G.; Dresselhaus, M.S. *Appl. Phys. Lett.* **2000**, *77*, 3161-3163.
(42) Vigolo, B., Penicaud, A.; Coulon, C.; Sauder, C.; Pailler, R.; Journet, C.; Bernier, P.; Poulin, P. *Science* **2000**, *290*, 1331-1334.
(43) Bethune, D. S., Kiang, C.H.; DeVries, M.; Gorman, G.; Savoy, R.; Vazquez, J.; Beyers, R. *Nature* **1993**, *363*, 605.
(44) Iijima, S., Ichihashi, T. *Nature* **1993**, *363*, 603-605.
(45) Cassell, A. M., Raymakers, J.A.; Kong, J.; Dai, Hongjie *J. Phys. Chem. B* **1999**, *103*, 6484-6492.
(46) Chiang, I. W.; Brinson, B. E.; Huang, P. A.; Willis, A.; Bronikowski, M. J.; Margrave, L.; Smalley, R. E.; Hauge, R. H. *J. Phys. Chem. B* **2001**, *105*, 8297-8301.
(47) Dillon, A. C., Gennett, T.; Jones, K. M.; Alleman, J. L.; Parilla, P. A.; Heben, M. J. *Adv. Mater.* **1999**, *11*, 1354-1358.
(48) O'Connell, M. J., Boul, P.; Ericson, L.M.; Huffman, C.; Wang, Y.; Haroz, E.; Kuper, C.; Tour, J.; Ausman, K.D.; Smalley, R.E. *Chem. Phys. Lett.* **2001**, *342*, 265-271.
(49) McCarthy, B., Coleman, J.N., Czerw, R., Dalton, A.B., Panhuis, M., Maiti, A., Drury, A., Bernier, P., Nagy, J.B., Lahr, B., Byrne, H.J., Carroll, D.L., Blau, W.J. *J. Phys. Chem. B* **2002**, *106*, 2210-2216.
(50) Kymakis, E., Amaratunga, G.A.J. *Appl. Phys. Lett.* **2002**, *80*, 112-114.
(51) Biercuk, M. J., Llaguno, M.C., Radosavljevic, M., Hyun, J.K., Johnson, A.T., Fischer, J.E. *Appl. Phys. Lett.* **2002**, *80*, 2767-2769.
(52) Qian, D., Dickey, E.C., Andrews, R. Rantell, T. *Appl. Phys. Lett.* **2000**, *76*, 2868-2870.
(53) Lau, K. *Carbon* **2002**, *1*.
(54) Ajayan, P. M., Schadler, L.S. *Adv. Mater.* **2000**, *12*, 750-753.
(55) Gong, X., Liu, J., Baskaran, S., Voise, R.D., Young, J.S. *Chem. Mater.* **2000**, *12*, 1049-1052.
(56) Wei, C., Srivastava, D., Cho, K. *Nanoletters* **2002**, *in press*.
(57) Liao, K., Li, S. *Appl. Phys. Lett.* **2001**, *79*, 4225-4227.
(58) de Heer, W. A., Bacsa, W.S., Chatelain, A., Gerfin, T., Humphrey-Baker, R., Forro, L., Ugarte, D. *Science* **1195**, *268*, 845-847.
(59) Hughes, M., Chen, G.Z., Shaffer, M.S.P., Fray, D.J., Windle, A.H. *Chem. Mater.* **2002**, *14*, 1610-1613.
(60) Tang, B. Z., Xu, H. *Macromolecules* **1999**, *32*, 2569-2576.
(61) Skoog, D. A.; Holler, F. J.; Nieman, T. A. *Principles of Instrumental Analysis*; 5th ed.; Saunders College Publishing: Philadelphia, 1998.
(62) Minami, N.; Kazaoui, S.; Jacquemin, R.; Yamawaki, H.; Aoki, K.; Kataura, H.; Achiba, Y. *Synth. Met.* **2001**, *116*, 405-409.
(63) Kazaoui, S.; Minami, N.; Kataura, H.; Achiba, Y. *Synth. Met.* **2001**, *121*, 1201-1202.
(64) Corio, P.; Temperini, M. L. A.; Santos, P. S.; Romero, J. V.; Huber, J. G.; Luengo, C. A.; Brown, S. D. M.; Dresselhaus, M. S.; Dresselhaus, G.; Dantas, M. S. S.; Leite, C. F.; Matinaga, F.; Gonzalez, J. C.; Pimenta, M. A. *Chem. Phys. Lett.* **2001**, *350*, 373-380.
(65) Wallace, J. M. In *Chemistry*; Rochester Institute of Technology: Rochester, 1994, pp 32-33.

(66) Souza Filho, A. G.; Jorio, A.; Dresselhaus, M. S.; Dresselhaus, G.; Saito, R.; Swan, A. K.; Unlu, M. S.; Goldberg, B. B.; Hafner, J. H.; Lieber, C. M.; Pimenta, M. A. *Phys. Rev. B* **2002**, *65*, 035404/035401.

(67) Thess, A.; Lee, R.; Nikolaev, P.; Dai, H.; Petit, P.; Robert, J.; Xu, C.; Lee, Y. H.; Kim, S. G.; Rinzler, A.; Colbert, D. T.; Scuseria, G.; Tomanek, D.; Fischer, J. E.; Smalley, R. *Science* **1996**, *273*, 483.

(68) Chiang, I. W.; Brinson, B. E.; Smalley, R. E.; Margrave, L.; Hauge, R. H. *J. Phys. Chem. B* **2001**, *105*, 1157-1161.

(69) Zhao, W.; Song, C.; Pehrsson, P. *J. Am. Chem. Soc.*, submitted for publication.

(70) Kazaoui, S.; Minami, N.; Yamawaki, H.; Aoki, K.; Kataura, H.; Achiba, Y. *Phys. Rev. B* **2000**, *62*, 1643–1646.

(71) Reich, S.; Thomsen, C.; Ordejon, P. *Phys. Rev. B* **2002**, *65*, 155411.

(72) Landi, B. J.; Raffaelle, R. P.; Gennet, T., In press.

(73) Landi, B. J.; Raffaelle, R. P.; Heben, M. J.; Alleman, J. L.; VanDerveer, W.; Gennett, T. *Nano. Lett.* **2002**, *2*, 1329-1332.